CaMKII binds both substrates and activators at the active site

Can Özden[1,2], Roman Sloutsky[1], Tomohiro Mitsugi[5], Nicholas Santos[1], Emily Agnello[1], Christl Gaubitz[4], Joshua Foster[2], Emily Lapinskas[1], Edward A. Esposito[3], Takeo Saneyoshi[5], Brian A. Kelch[4], Scott C. Garman[1], Yasunori Hayashi[5], Margaret M. Stratton[1]†

[1]Department of Biochemistry and Molecular Biology, University of Massachusetts, Amherst, MA 01003, USA. [2]Molecular and Cellular Biology Graduate Program, University of Massachusetts, Amherst, MA 01003, USA. [3]Malvern Panalytical, Northampton, MA 01060, [4]Department of Biochemistry and Molecular Biotechnology, University of Massachusetts Chan Medical School, Worcester, MA 01605, USA. [5]Department of Pharmacology, Kyoto University Graduate School of Medicine, Kyoto, 606-8501 Japan.

† Corresponding author. Email: mstratton@umass.edu (M.M.S.)

ABSTRACT

Ca^{2+}/calmodulin dependent protein kinase II (CaMKII) is a signaling protein required for long-term memory. Once activated by Ca^{2+}/CaM, it sustains activity even after the Ca^{2+} dissipates. In addition to well-known autophosphorylation-mediated mechanism, interaction with specific binding partners also persistently activates CaMKII. A longstanding model invokes two distinct S- and T-sites. If an interactor binds at the T-site, it will preclude autoinhibition and allow substrates to be phosphorylated at the S-site. Here, we specifically test this model with X-ray crystallography, molecular dynamics simulations, and biochemistry. Our data are inconsistent with this model. Co-crystal structures of four different activators or substrates show that they all bind to a single continuous site across the kinase domain. We propose a mechanistic model that persistent CaMKII activity is facilitated by high affinity binding partners, which kinetically compete with autoinhibition by the regulatory segment to allow substrate phosphorylation.

KEYWORDS

Ca^{2+}/calmodulin dependent protein kinase II, X-ray crystallography, NMDA-type glutamate receptor, AMPA-type glutamate receptor, T-lymphoma invasion and metastasis-inducing protein 1

INTRODUCTION

Ca^{2+}/calmodulin-dependent protein kinase II (CaMKII) is a central signaling protein that controls cellular functions such as synaptic plasticity, cytoskeletal regulation, cell growth and division, gene transcription, and ion channel modulation [1]. CaMKII biology has been an active focus of research especially because of its crucial role in long-term potentiation (LTP), which is the basis for long-term memory [2, 3]. CaMKII is highly abundant in the forebrain postsynaptic density (PSD) fraction, where it makes up to 2% of the total protein [4]. CaMKII is a multisubunit complex made up of 12-14 subunits, which is oligomerized by the hub domain (**Fig. 1A**). Each CaMKII subunit contains a Ser/Thr kinase domain, autoinhibitory/regulatory segment, variable linker region, and a hub domain (**Fig. 1B**). CaMKII is governed by many molecular interactions, however, the structural details of these interactions are lacking (**Fig. 1C**) [5].

Ca^{2+}/calmodulin (Ca^{2+}/CaM) activates CaMKII by binding to the regulatory segment and thereby freeing the substrate binding site. This well-understood mechanism triggers trans-autophosphorylation of T286, which renders CaMKII constitutively active until T286 is

dephosphorylated. CaMKII has also been shown to maintain activity in the absence of Ca^{2+}/CaM and T286 phosphorylation by another mechanism that invokes binding partners [6-9], for which we lack a clear mechanism. There are three binding partners (NMDA receptor, Tiam1, and *Drosophila* EAG (*d*EAG)) that have been shown to be activators of CaMKII after the Ca^{2+} stimulus dissipates, with or without T286 phosphorylation [7-10]. The GluN2B subunit of the NMDA receptor is a known substrate of CaMKII [11, 12], and to this point, is the best studied CaMKII activator [13]. Ca^{2+}/CaM-activated CaMKII has been shown to form a persistent complex with GluN2B, which locks CaMKII in an active conformation, as long as binding persists [7, 12]. Persistent binding of CaMKII to GluN2B and resultant activation has been explained by a hypothetical model [8]. In this model, GluN2B first binds to Ca^{2+}/CaM-activated CaMKII close to the active site (termed S-site), presenting Ser 1303 for phosphorylation. Then, GluN2B dissociates from CaMKII and then re-binds at the base of the CaMKII C-lobe (termed T-site), while freeing the S-site to bind and phosphorylate other substrates. This model has been widely accepted in the field, but to date, there is no structural data supporting it.

Another known activator is Tiam1, a Rac guanine-nucleotide exchange factor (RacGEF), and it is phosphorylated multiple sites by CaMKII. The carboxy tail of Tiam1 also forms a stable complex with CaMKII using a pseudosubstrate sequence (alanine at the phosphorylation site) [9]. The third activator is *d*EAG, a potassium channel in *Drosophila* [10]. Both Tiam1 and *d*EAG behave similarly to GluN2B in that binding maintains CaMKII activation in the absence of Ca^{2+}/CaM [9, 10]. A recent structure shows that *d*EAG binds over an extensive surface on the CaMKII kinase domain [14]. On the other hand, densin-180 (LRRC7) is a postsynaptic scaffolding protein. It also forms a stable complex with CaMKII through a pseudosubstrate sequence (isoleucine at the phosphorylation site), but unlike GluN2B or Tiam1, it inhibits kinase activity selectively [15, 16]. Finally, the AMPA receptor subunit GluA1 is a CaMKII substrate but not a known activator [17, 18]. GluA1 phosphorylation by CaMKII is important for synaptic plasticity [19-21].

In the current study, we solved co-crystal structures of the CaMKII kinase domain bound to peptides from GluN2B, Tiam1, densin-180, and GluA1. Using these structures as starting points, we compared molecular dynamics (MD) simulations of the kinase domain in complex with GluN2B, Tiam1, and a previously solved structure with CaMKII bound to an inhibitor, CaMKIIN [22]. Combining this structural information with the biophysical and biochemical measurements has allowed us to clarify important interactions that drive binding and propose a working model for maintaining CaMKII activity in the absence of Ca^{2+}/CaM.

RESULTS

The studies outlined below include co-crystallization of the CaMKII kinase domain bound to peptides from the following CaMKII binding partners: GluN2B (residues 1289-1310), GluA1 (residues 818-837), densin-180 (residues 797-818), and Tiam1 (residues 1541-1559). We also include CaMKIIN in these studies, which is a known endogenous inhibitor of CaMKII [23-25]. Unless otherwise specified, all experiments were conducted in the background of an inactivating CaMKII mutation (D135N). This mutation effectively disables kinase activity by removing the catalytic base while preserving the structural integrity of the kinase. Indeed, an overlay of the wild-type (WT) kinase domain with the D135N kinase domain structure shows very few deviations (root-mean-square deviation (RMSD) = 0.309).

In addition to analysis of the crystal structures, we also performed MD simulations of the kinase domain in complex with extended versions of peptides to assess any contributions from the terminal ends that would not be observed in the crystal structures. All simulations were

101 performed in the NPT ensemble at 300K. One production simulation was performed for the
102 kinase:GluN2B and kinase:Tiam1 complexes, producing trajectories of 2.19 μs and 2.05 μs,
103 respectively. Two independent simulations were performed for the kinase:CaMKIIN complex.
104 These were 0.46 μs and 1.84 μs in length, for an aggregate of 2.3 μs. RMSD and root-mean-
105 square fluctuation (RMSF) for the kinase domain and the peptide were calculated over the
106 course of the trajectories (**Fig. S1A-C**).
107
108 **CaMKII kinase domain has a single binding site**
109 We first used isothermal titration calorimetry (ITC) to measure binding affinity of peptides to the
110 CaMKII kinase domain (D135N). We showed that four out of five peptides bound to the kinase
111 with high affinity, whereas GluA1 bound with significantly lower affinity (**Fig. 2A-E**). The K_d
112 values for single-site binding ranged from 39 nM to >55 μM (GluN2B K_d = 107±47 nM, CaMKIIN
113 K_d = 39±24 nM, densin-180 K_d = 585±114 nM, Tiam1 K_d = 1.1±0.1 μM, GluA1 K_d >55 μM)
114 (**Table 4**). From these data, it appears that GluA1 is the outlier whereas the other partners bind
115 with relatively high affinity.
116
117 We then determined 12 total crystal structures of the CaMKII kinase domain (residues 7-274,
118 lacking the regulatory domain) bound to one of four peptides: GluN2B, GluA1, densin-180, and
119 Tiam1 (**Fig. 2F, S2A-D)**). We resolved 14-19 residues in each peptide. All structures have
120 resolutions within the range of 1.85 – 3.1 Å (**Tables 1-3**). We solved eight structures of the
121 kinase domain bound to the GluN2B peptide (WT and phosphomimetic S1303D) with different
122 ligands in the nucleotide binding pocket (**Tables 1,2**). We also solved structures of the kinase
123 domain bound to peptides of Tiam1, densin-180, and GluA1, with ATP bound or empty
124 nucleotide binding pockets (**Table 3**). Of note, in a structure with both ATP and S1303D GluN2B
125 bound (PDB: 7KL1), there is strong density between the aspartate side chain and gamma
126 phosphate group, indicating the formation of a covalent bond similar to what would be expected
127 for transfer of the gamma phosphate to the carboxylate (**Fig. S2E**).
128
129 Across all structures, we observed that peptides interacted with the same surface on the kinase
130 domain. The overall fold of the kinase domain is similar in all structures. So far, predicting
131 CaMKII interaction partners has been difficult due to conformational heterogeneity. Our
132 structures revealed that several peptides have helical turns, which shifted the register of
133 conserved interactions. In the CaMKIIN structure, there is an internal short helical turn [22].
134 Tiam1 and GluA1 peptides also adopted short helical turns, however they were shifted to the
135 proximal (N-terminal) end compared to CaMKIIN. GluN2B and densin-180 peptides bound in
136 completely extended conformations with no helical turns. We now provide an updated sequence
137 alignment based on our structural observations (numbering is based on the prototypical GluN2B
138 substrate with the phosphorylation site set to zero and the inserted residues are not counted)
139 (**Fig. 2G**). The two peptides that are substrates (GluN2B and GluA1) have the phosphosite
140 facing the nucleotide binding pocket, such that both peptides are docked at the active site,
141 ready to be phosphorylated. The critical residues of the binding partner mediating this
142 interaction are conserved at positions +1, -2, -3, -5, and -8, which are discussed in detail below
143 (**Fig. 3**).
144
145 **Interactions driving binding to the CaMKII kinase domain**
146 Hydrophobic residue the +1 position. Our alignment is consistent with previous studies showing
147 that a small hydrophobic residue is preferred at the +1 position [14, 26-29] (**Fig. 2G**). Our
148 structures revealed a hydrophobic patch adjacent to G175 in the kinase domain forms a docking
149 site for small and medium sized hydrophobic residues (valine, isoleucine, and leucine) (**Fig.
150 3A**). In GluN2B, tyrosine is larger and polar, so the sidechain is not buried in the hydrophobic

151 pocket unlike the other binding partners. In all structures, backbone atoms of the +1 position
152 forms hydrogen bond with the backbone of G175.
153
154 In the Tiam1 crystal structure, the +1 leucine does not interact with this groove. We
155 hypothesized that this is because it is the C-terminal residue on the peptide used for
156 crystallization. To test this, we extended the Tiam1 sequence and performed MD simulations,
157 which showed that the +1 leucine does interact with the hydrophobic patch. In the simulations,
158 we observed that the +1 leucine and also the +4 isoleucine interact strongly over the course of
159 the trajectory with an average distance of 3.2 Å (**Fig. S3A**). We compared this to simulations of
160 GluN2B and CaMKIIN, which also show a relatively strong interaction between the +1 residue
161 and the hydrophobic patch (**Fig. S3B, C**). In both GluN2B and Tiam1, the +1 residue fluctuates
162 in and out of the pocket, as shown by the larger distribution of distance from the pocket.
163 Additionally, the +4 residue of GluN2B is also strongly interacting with the pocket similar to
164 Tiam1 whereas the CaMKIIN +2 residue is interacting less.
165
166 Ionic interactions at the -2 position. Glutamine is commonly found at the -2 position of CaMKII
167 interactors [14, 26-28]. Indeed, all four peptides in our structures have glutamine at -2, allowing
168 us to resolve the important interactions mediated by both the backbone and the sidechain at this
169 position. There is extensive hydrogen bonding between the -2 glutamine and G178, Y179,
170 K137, and E139 (**Fig. 3B**). CaMKIIN has a serine at the -2 position and the side chain is flipped
171 relative to glutamine, which enables tighter interactions with E139 and K137 side chains [22].
172 This observation is consistent with a previous study, which showed that CaMKIIN binding to
173 CaMKII was reduced when this serine was mutated to alanine [30].
174
175 Conserved salt bridge at the -3 position. Like many kinases, CaMKII prefers a basic residue at
176 the -3 position [31]. In the crystal structures, all interactors except for the low-affinity binder
177 GluA1 have a basic residue at the -3 position (arginine or lysine), which forms salt bridges with
178 two glutamic acid residues (E96, E99) located on the αD helix of the kinase domain (**Fig. 3C,**
179 **4A**) [14, 22, 32, 33]. These salt bridges are not formed with GluA1, because there is a proline at
180 the -3 position. In the GluA1 structure, the sidechain of E96 is flipped away from the peptide
181 compared to the other four structures where it is oriented toward the binding partner (**Fig. 4A**,
182 inset).
183
184 We hypothesized that the reason for GluA1's lower affinity was due to the lack of these salt
185 bridges. To test this, we measured binding of a mutant GluA1 peptide where the -3 proline was
186 changed to an arginine (GluA1 P828R). This mutation increased binding >140-fold to K_d = 376
187 nM (**Fig. 4B**). To further validate this, we created single and double charge reversal mutations
188 (E→K) and compared the behavior of GluA1 P828R to a high affinity interactor, GluN2B. Single
189 mutants (E96K or E99K) decreased the affinity to both GluA1 P828R and GluN2B by 7- to 65-
190 fold, whereas the double mutant (E96/99K) decreased affinity by 75- to 140-fold (**Fig. S4, S5,**
191 **Tables 4, 5**). These data indicate the importance of these salt bridges in determining binding
192 affinity.
193
194 We also wanted to investigate the role of E96/99 in ATP binding. E96 is well-conserved across
195 kinases and known to be important for ATP binding [33]. Almost 50% of kinases have either an
196 aspartate or glutamate at this position (E96), which might explain the basophilic kinase
197 substrate preference [34]. In structures where ATP/Mg^{2+} is bound (GluN2B, Tiam1), the side
198 chain of E96 interacts with the hydroxyl groups of ribose in ATP (**Fig. S6A**). In MD simulations
199 with CaMKIIN, interactions with ATP were very different. We observed a unique interaction at
200 the -3 position, which resulted in a conformation that distorted ATP binding (**Fig. S6B**). MD
201 trajectories predict that CaMKIIN binding is facilitated by E96 in the presence of ATP, whereas

202 E99 plays essentially no role. We performed ITC measurements comparing binding of CaMKIIN
203 to the kinase domain with charge reversal mutations (E96K, E99K) in the presence of an
204 unhydrolyzable ATP analogue (AMP-PNP). Consistent with the prediction from the simulation,
205 the affinity of E99K was only 2-fold weakened while E96K weakened by 10-fold (**Fig. S4, S6C-**
206 **F, Table 5**). Further efforts will need to interrogate the role of ATP coordination in CaMKIIN
207 inhibition. E99 is not as well-conserved, even across other CaM-kinases (**Fig. S7A-C**),
208 indicating that it may be more important for substrate specificity and potentially compensate if
209 E96 is mutated [35].
210
211 Hydrophobic interaction at the -5 position. All CaMKII interactors studied here have a conserved
212 leucine at the -5 position, which fits into a hydrophobic pocket on the kinase domain comprised
213 of F98, I101, V102, and I205 (**Fig. 3D, 5A**). In these structures, leucine is 3.3-4.5 Å from the
214 four hydrophobic residues, indicating a tight interaction as compared by measuring the distance
215 between the closest carbon atoms in each residue. In the CaMKIIN structure, a turn motif,
216 facilitated by two glycines, orients leucine at the -8 position into this pocket to make it nominally
217 at the -5 position [22]. In simulations of GluN2B, Tiam1, and CaMKIIN, this interaction also
218 demonstrates high structural integrity, with pairwise RMSD below 2 Å (**Fig. 5B**).
219
220 Docking site mediated by W214. In both densin-180 and CaMKIIN structures, the sidechains of
221 proline and isoleucine (highlighted blue in **Fig. 2G**) pack against W214 on the kinase domain
222 (**Fig. 5C**). For densin-180, the guanidino group of R808 at the -7 position hydrogen bonds with
223 the backbone carbonyl group of W214 and the sidechain of Q224. In simulations of CaMKIIN,
224 the pairwise RMSD calculated for W214 interacting with isoleucine and proline below 1.5 Å,
225 indicating a strong and persistent interaction over the course of the trajectory (**Fig. 5D).**
226
227 We measured binding to a kinase domain mutated at this tryptophan (W214A) to discern its
228 contribution to these interactions. The W214A mutation significantly disrupted CaMKIIN binding
229 by lowering the affinity 60-fold, whereas the effects on the other binding partners were not as
230 severe (4- to 10-fold decreased affinity) (**Fig. 5E, Fig. S8A-D, Tables 4, 5**). CaMKIIN docking
231 onto W214 likely stabilizes its helical motif, which properly orients the -5 leucine into the
232 hydrophobic pocket. When W214 is mutated, the -5 leucine interaction is unlikely to be
233 maintained in CaMKIIN, which results in disrupted binding. Densin-180 does not have a helical
234 motif, which may explain why the W214A mutant does not have a drastic effect on binding.
235 CaMKIIN has been characterized as a CaMKII specific inhibitor despite the fact that CaMKII has
236 high similarity to the CaMK-family kinases. This specificity is likely driven by the presence of this
237 tryptophan residue as the other family members have tyrosine or methionine at this position
238 (**Fig. S7A**).
239
240 Salt bridge at the -8 position. We observed a novel electrostatic interaction between a
241 conserved basic residue at the -8 position (arginine or lysine) and a glutamate (E236) at the
242 base of the C-lobe (**Fig. 3E, 6A**). This has not been previously described likely because this
243 position is quite far from the phosphorylation site (~30 Å), and substrate alignments have not
244 been accurate enough to highlight the conservation at this position. We tested the effect of
245 mutating E236 to lysine (E236K) on binding affinity. The E236K mutation completely abolished
246 Tiam1 binding (**Fig. 6B, Fig. S8E, Table 5**). For densin-180, CaMKIIN, and GluN2B, E236K
247 binding affinity was reduced ~17-fold (K_d = 10±7 μM), ~21-fold (K_d = 825±6 nM) and ~35-fold (K_d
248 = 3.5±1 μM), respectively (**Fig. 6B, Fig. S8F-H, Tables 4, 5)**. Previous work noted that E236K
249 did not significantly affect GluN2B binding in biochemical assays [8], however, in that
250 measurement low micromolar binding would not be discernable from high nanomolar binding as
251 in our ITC measurements.
252

253 We wondered whether substrate phosphorylation would alter this interaction that is so far from
254 the active site. To test this, we measured the affinity between the E236K kinase domain and the
255 phosphomimetic GluN2B (S1303D, S→D at position 0). There was very little effect on the
256 S1303D GluN2B binding to D135N (K_d = 493±47 nM) (**Fig. S9A**), whereas affinity for the E236K
257 mutant was reduced ~24-fold (K_d = 12±4.5 μM) (**Fig. 6B, Fig. S9B, Table 4**). This indicates that
258 E236K significantly weakens binding to S1303D GluN2B.
259
260 **Generalizing CaMKII binding partners**
261 We mined the curated database of CaMKII phosphorylation sites (n=418) for consistencies with
262 our updated alignment and found additional similarities (**Fig. S7D**, www.phosphosite.org) [40].
263 Hydrophobic residues (I, V, L, M, F) are found at +1, Q is found at -2, and R is overwhelmingly
264 found at -3, but also at -2 and -4. Smaller hydrophobic residues (L, V, I, M) are found at -5 and -
265 6. Generally, the minus direction disfavors P, D, and E. In contrast, acidic residues D and E are
266 highly favored at +2. GluN2B has D at the +2 position, and we note an interaction with K56 in
267 several structures, which was also observed in the *d*EAG-bound structure (PDB: 5H9B) [14]. In
268 addition, S, which may serve as a second phosphorylation site, is strongly disfavored at nearly
269 every position. The Phosphosite Plus database only allows analysis out to +7/-7 positions so we
270 could not compare residues at the -8 position and beyond. The actual -8 position may be farther
271 than anticipated from alignments due to secondary structural elements. Overall, these features
272 are consistent with important residues identified in our structures.
273
274 **Interrogating CaMKII interactions with full-length binding partners**
275 In order to assess the importance of the residues on CaMKII identified in the crystallographic
276 analysis, we used a pull-down assay to assess the effect of CaMKII mutations on interactions
277 with full-length binding partners. We co-transfected HEK293 cells with FLAG-tagged full-length
278 CaMKIIα and either full-length Tiam1, GluN2B, or GFP-CaMKIIN. Binding was assessed by
279 western blot following immunoprecipitation with an anti-FLAG antibody. Immunoprecipitation
280 showed a remarkable loss of binding for both Tiam1 and GluN2B when E236 is mutated, similar
281 to our ITC data (**Fig. 6C, D**). E236K CaMKII resulted in better binding to CaMKIIN compared to
282 WT CaMKII in HEK293 cells (**Fig. 6E**). Our ITC results showed tight binding between the E236K
283 CaMKII kinase domain and CaMKIIN (825 nM), and it is known that the E236K mutation
284 disrupts regulatory segment binding [32], thereby facilitating more CaMKIIN binding to E236K
285 compared to WT since the binding site is more available. The far salt bridge interaction
286 mediated by E236 facilitates high affinity binding to CaMKII and may also be critical for CaMKII
287 specificity as it is not conserved across other CaMK-family kinases.
288
289 The immunoprecipitation experiments also corroborate our peptide binding data that show the
290 importance of hydrophobic interactions. Indeed, mutating the hydrophobic pocket at the -5
291 position (I205K) showed significant loss of CaMKII binding to Tiam1, GluN2B, and CaMKIIN
292 (**Fig. 6C-E**). The W214A mutation also disrupted binding to Tiam1, GluN2B, and CaMKIIN. The
293 pull-down assay revealed a significant effect on Tiam1 binding to W214A, which is in agreement
294 with ~9-fold lower affinity from ITC measurements (**Fig. 6C**). The W214A mutation slightly
295 weakened the interaction with full-length GluN2B, and we observed 4-fold lower affinity in our
296 ITC measurement using GluN2B peptide (**Fig 6D**). Consistent with our ITC data, CaMKIIN
297 binding to W214A was remarkably weakened compared to WT (**Fig. 6E**). CaMKIIN is a high
298 affinity inhibitor of CaMKII, and its specificity likely arises from this W214 docking site which is
299 not present in other CaMK-family members (**Fig. S7A, C**). In this way, W214 might serve as a
300 docking site for CaMKII-specific interactions. Additionally, a previous study suggested that the
301 pantothenate segment of Coenzyme A packs against W214 of CaMKII to mediate this
302 interaction [41].
303

304 **The αD helix rotates outward to accommodate binding partners**
305 CaMKII is unique among protein kinases in that it does not require phosphorylation in the
306 activation loop. In fact, CaMKII structures have highlighted that the autoinhibited conformation of
307 CaMKII actually resembles many other kinases' active conformations [36, 37]. Upon activation,
308 the αD helix in CaMKII undergoes a 45° rotation outward [33, 36, 38]. In the autoinhibited
309 conformation, the regulatory segment stabilizes the αD helix in the inward conformation [36].
310
311 We then compared the structures of autoinhibited kinase (PDB:2VZ6, residues 13-300) [33], the
312 uninhibited kinase (PDB:6VZK) [39], and the kinase bound to GluN2B. It is clear from this
313 comparison that that the αD helix rotates outward to accommodate GluN2B binding, just as it
314 does when the regulatory segment is removed (**Fig. 7A**). This is also true for Tiam1, GluA1,
315 densin-180, and CaMKIIN [22]. The rotation of the αD helix effectively presents the hydrophobic
316 patch in a competent position for interacting with the binding partner. The αD helix houses three
317 of the four residues that make up the hydrophobic pocket for the -5 leucine to dock in, which is
318 likely a large contribution to an observed gain in kinase domain stability upon substrate binding
319 [6] (**Fig. S10A**), similar to what we have previously observed with regulatory segment binding,
320 which is mediated by L290 in the regulatory segment [39].
321
322 **Testing the S- and T-site binding model**
323 Since our structures revealed that all interactors bound to the same single site on the kinase
324 domain, we wanted to directly test the idea of the 2-site (S- and T-site) binding model [8].
325 Previous studies have shown that GluN2B peptide could not be competed off by Syntide-2 even
326 at low millimolar concentrations, which we also observed (**Fig. 7B**) [12]. As noted by Colbran
327 and colleagues [12], a sequence alignment of Syntide-2 compared to other substrates reveals
328 that the Syntide-2 peptide is shorter at the N-terminus and is therefore missing the -8 position
329 basic residue necessary for mediating the far salt bridge. To test whether this is the reason
330 Syntide-2 could not compete GluN2B, we created an extended version of Syntide-2 by adding
331 three residues to the N-terminus, mimicking densin-180 (**Fig. 7B**, inset). The extended version
332 of Syntide-2 did compete off GluN2B (K_i ~ 78±14 μM) (**Fig. 7B**). This result shows that Syntide-
333 2 and GluN2B occupy the same binding site, indicating that there are not two separate binding
334 sites on the kinase domain. When we tried to measure affinity for Syntide-2 peptide using ITC,
335 we did not see any appreciable binding despite using protein/peptide concentrations high
336 enough to characterize an interaction with a K_d of several hundred micromolar (**Fig. S11**). When
337 we tested the extended version of Syntide-2 in ITC, we obtained a K_d of 2.6±0.9 μM **Fig. S11**,
338 providing further evidence that this far salt bridge at the -8 position facilitates tight binding.
339
340 A conundrum thus arises: if there are not two distinct binding sites, how is CaMKII activity
341 maintained by specific binding partners like GluN2B? The mode of activation must invoke the
342 phosphorylated form of GluN2B since this is observed under activating conditions. In a
343 canonical kinase reaction, the kinase first binds substrate and ATP, then transphosphorylation
344 occurs, and finally the substrate is released and ADP is replaced by another ATP molecule. We
345 measured the affinity of the phosphomimetic GluN2B peptide (S1303D) (K_d = 493±47 nM) and
346 observed only a ~5-fold reduction in affinity compared to WT GluN2B (K_d = 107±46 nM) (**Fig.**
347 **S9A, 2B**). In the presence of AMPPNP, there is also tight binding of S1303D GluN2B (K_d =
348 277±30) (**Fig. S9C**). We were also able to crystallize the kinase domain bound to GluN2B
349 S1303D, which showed the same conformation as bound to WT GluN2B (backbone RMSD
350 0.266 Å) (**Fig. S10B**). We hypothesized that phospho-GluN2B would act as a competitive
351 inhibitor for Syntide-2 due to this tight binding. We performed kinase assays using Syntide-2 as
352 a substrate in the presence of saturating GluN2B S1303D. As a control, we also measured
353 activity against Syntide-2 in the presence of the CaMKIIN. Indeed, high levels of CaMKIIN
354 completely inhibit Syntide-2 phosphorylation, whereas GluN2B acts as a competitive inhibitor,

355 exemplified by comparable V_{max} values but an increased K_m value (**Fig. 7C**). These data
356 indicate that GluN2B and Syntide-2 bind to the same site.
357
358 **A proposed model for persistent CaMKII activity**
359 Based on our data, we propose a mechanistic model to explain the observations of prolonged
360 CaMKII activity in the presence of specific binding partners. Let's consider the mode of
361 activation by GluN2B as the activator shown in **Figure 7D**. As described above, upon Ca^{2+}/CaM
362 binding and release of autoinhibition, the kinase domain undergoes a conformational change
363 where the αD helix rotates out and the kinase is in the 'on' state (**Fig. 7A**). Following
364 dissociation of GluN2B, a conformational change in the αD helix is required for the regulatory
365 segment to re-bind but not for a new substrate to bind. For this reason, we hypothesize that
366 under conditions of high substrate concentrations, substrate binding will be faster than
367 regulatory segment re-binding. In conditions where the activator concentration is high, activator
368 rebinding will be favorable since this high affinity binder will have a relatively high on-rate and
369 low off-rate.
370
371 **DISCUSSION**
372 CaMKII recognizes a broad range of interaction partners, yet the structural details driving these
373 interactions had not been elucidated. We addressed this by solving co-crystal structures of four
374 binding partners bound to the CaMKII kinase domain, which allowed us to highlight the
375 interactions mediating binding. The minimum consensus sequence for CaMKII targets is R-X-X-
376 S/T [42, 43], however, our results have expanded upon this understanding. If we incorporate our
377 structural observations, the full consensus sequence is: R/K-X-X-ϕ-X-R/K-X-X-S/T-ϕ. We
378 postulate that if all positions are satisfied as shown here, the binding affinity will be high
379 nanomolar to low micromolar. Interaction partners lacking 1-2 of these positions will have poorer
380 affinities but may still be viable interactors, since a typical kinase substrate has an affinity of
381 several hundred micromolar [44]. For example, GluA1 lacks a basic residue at the -3 position
382 which yields an affinity of >55 μM. The biological ramifications of the weak interaction between
383 CaMKII and GluA1 will need to be further investigated – where localization of CaMKII to this
384 receptor by another factor or avidity effects of holoenzyme localization may be driving GluA1
385 phosphorylation *in vivo* [45]. Our observation might explain the molecular basis of a recent study
386 that reported lower levels of S831 phosphorylation in the hippocampus [46]. We report GluA1 as
387 a low-affinity substrate, which would explain why densin-180 was interpreted as a selective
388 inhibitor since GluA1 would not be strong enough to compete with densin-180 binding [16].
389 Given the large size and scaffolding role of densin-180 (180 kDa) compared to CaMKIIN, the
390 densin-180 interaction might be more important for CaMKII localization than widespread
391 inhibition.
392
393 There has been a lack of mechanistic clarity in understanding how certain CaMKII interactors
394 lead to prolonged activation in the absence of calcium. In 2001, without a crystal structure to
395 guide an understanding, a set of extraordinary data revealed that GluN2B binding yielded
396 autonomous CaMKII activity [7]. This work came on the heels of an extensive mutagenesis
397 study mapping how the regulatory domain interacts with the surface of the kinase [32]. One of
398 the findings from this work was that the mechanism of autoinhibition is distinct from substrate
399 binding, especially when residues far from the active site were tested. To orient thinking about
400 these interactions, residues close to the active site were termed the S-site (for substrate
401 binding) and residues far from the active site were termed the T-site (for Thr286 binding) [38,
402 47]. In 2006, these reference points were implemented into a 2-site binding model to explain this
403 autonomous activity with GluN2B binding [8].
404

We were well-poised to systematically test the S- and T-site model using biochemistry and structural biology. In the described model, F98 is part of the S-site and I205 is part of the T-site [8]. Conversely, we find that all interactors, including activators, bind to the CaMKII kinase domain using a continuous single site across the surface of the kinase domain [14, 22]. In these structures, F98 and I205 (along with I101 and V102) make up a single hydrophobic pocket that houses the -5 leucine residue, first described by Kuriyan and colleagues as 'docking site B' (**Fig. 3D, 5A**) [22]. So, F98 and I205 are performing the same role, instead of comprising separate sites. A large body of evidence for the S- and T-site model has been based on experiments that compare a short synthetic substrate Syntide-2 (lacks a basic residue at the -8 position) to another substrate AC3 (contains a -8 basic residue). Syntide-2 has been deemed an S-site binder whereas AC3 binds to both the S- and T-site. This distinction stemmed from data showing that if CaMKII is bound to Syntide-2 or AC3 and then GluN2B is added, GluN2B binds the CaMKII-syntide-2 but not the CaMKII-AC3 [8]. These data were interpreted such that GluN2B was able to bind to the T-site while Syntide-2 remained bound at the S-site. Based on our data, an updated interpretation is that GluN2B competes off Syntide-2 because GluN2B binds CaMKII with >1000-fold higher affinity.

CaMKII has high affinity (submicromolar to low micromolar) for activator peptides GluN2B, Tiam1, and *d*EAG [14]. This is somewhat unique, since typically these interactions are in the K_d range of 200 μM [44]. We postulate that these high affinity interactors allow the interaction partners to kinetically compete with regulatory segment rebinding by stabilizing the active conformation with the αD helix rotated outward. In conditions where substrate concentration is high, CaMKII will phosphorylate substrate because the kinase is in the active conformation and is in the proper conformation to interact with substrates. The data presented here provide clarity on the interactions between CaMKII and its binding partners, which will be crucial in guiding biological experiments to assess the downstream effects of specific interactions. Future experiments will necessarily invoke the complexities of the CaMKII holoenzyme structure. CaMKII-activator binding provides a mechanism to maintain CaMKII activity in the absence of Ca^{2+}. It is intriguing to consider other enzymes that might be modulated in a similar way by high affinity binding partners as a novel mechanism for prolonged activation in the absence of other stimuli.

MATERIALS AND METHODS

Cloning

All CaMKIIα variants were expressed with an N-terminal His-SUMO tag in a pET vector. For mammalian expression, CaMKIIα was expressed with a C-terminal Flag tag in pDEST12.2 vector [9]. Tiam1-mGFP was subcloned in a pCAGGS [9], GluN2B was in pGW-CMV (Kim et al., 1996, https://doi.org/10.1016/S0896-6273(00)80284-6), CaMKIIN-GFP was in pEGFP vector [25], and mCherry-Flag was in pDEST12.2 vector [9]. All point mutations were created using site-directed mutagenesis.

Protein Expression and Purification

WT CaMKIIα kinase domain (residues 7-274) was co-expressed with λ phosphatase in *E. coli* BL21(DE3). Inactive constructs (D135N) and CaMKIIN2 *(Rattus norvegicus)* were expressed without λ phosphatase. The cells were induced at 18 °C with 1 mM isopropyl β-a-D-1-thiogalactopyranoside (IPTG) and grown overnight. Following to ~16 hours incubation, cell pellets were resuspended in Buffer A (25 mM Tris, pH 8.5, 50 mM KCl, 40 mM imidazole, 10% glycerol) and commercially available protease inhibitors (0.5 mM benzamidine, 0.2 mM 4-(2-aminoethyl)benzenesulfonyl fluoride hydrochloride (AEBSF), 0.1 mg/mL trypsin inhibitor, 0.005 mM leupeptin, 1 μg/mL pepstatin), 1 μg/mL DNase/50 mM $MgCl_2$ were added, then lysed. All

following purification steps were performed using an ÄKTA pure chromatography system at 4 °C. Filtered cell lysate was loaded onto a 5 mL His Trap FF Ni Sepharose column (GE Research), and eluted with 50% Buffer B (25 mM Tris-HCl pH 8.5, 150 mM KCl, 1 M imidazole, 10% glycerol). The protein was desalted from excess imidazole using a HiPrep 26/10 Desalting column using Buffer C (25 mM Tris-HCl pH 8.5, 40 mM KCl, 40 mM imidazole, 2 mM tris(2-carboxyethyl)phosphine (TCEP), 10% glycerol). His SUMO tags were cleaved with Ulp1 protease overnight at 4 °C. Cleaved His SUMO tags were separated by a subtractive NiNTA step prior to an anion exchange step. Proteins were eluted from HiTrap Q-FF with a KCl gradient. Eluted proteins were concentrated and further purified in gel filtration buffer (25 mM Tris-HCl pH 8.0, 150 mM KCl, 1 mM TCEP, 10% glycerol) using Superdex 75 10/300 GL size exclusion column. Fractions (>95% purity) were pooled, concentrated, aliquoted and flash frozen in liquid nitrogen, and stored at -80 °C until needed.

We use rat full-length CaMKIIN2 protein in our ITC measurements, coupled-kinase assays and cellular immunoprecipitation experiments. The CaMKII-bound CaMKIIN co-crystal structure (PDB:3KL8) was obtained by using a peptide derived from rat CaMKIIN1. In our MD simulations, the full length human CaMKIIN1 amino acid sequence was used. Amino acid sequences of each construct are listed below:
CaMKIIN2 (*Rattus norvegicus*):
MSEILPYGEDKMGRFGADPEGSDLSFSCRLQDTNSFFAGNQAKRPPKLGQIGRAKRVVIEDDR
IDDVLKGMGEKPPSGV

CaMKIIN1 peptide (*Rattus norvegicus*):
KRPPKLGQIGRSKRVVIA

CaMKIIN1 (*Homo sapiens*):
MSEVLPYGDEKLSPYGDGGDVGQIFSCRLQDTNNFFGAGQNKRPPKLGQIGRSKRVVIEDDRI
DDVLKNMTDKAPPGV

Peptide synthesis
Peptides used for co-crystallization were synthesized and amidated at the C-terminus (Genscript, RIKEN Research Resource Center). Peptide used for fluorescence polarization assays were synthesized with an additional N-terminal 5-FAM.

Full length peptide sequences are as follows:
Human GluA1 (residues 818-837): SKRMKGFCLIPQQSINEAIR [Numbering for GluA1 is for mature peptide, excluding 18 amino acid long signal peptide, following convention in the field.]
Human GluN2B (residues 1289-1310): KAQKKNRNKLRRQHSYDTFVDL
Human GluN2B(S1303D) (residues 1289-1310): KAQKKNRNKLRRQHDYDTFVDL
Human densin-180 (residues 797-818): SKSRSTSSHGRRPLIRQDRIVG
Mouse Tiam1 (residues 1541-1559): RTLDSHASRMTQLKKQAAL
Syntide-2: PLARTLSVAGLPGKK
Extended Syntide-2: GRRPLARTLSVAGLPGKK

Full length peptide sequence for fluorescence polarization assays are as follows:
Human GluN2B(S1303D) (residues 1289-1310): KAQKKNRNKLRRQHDYDTFVDL

Crystallization and X-Ray Data Collection
Initial crystallization screening was done using the sitting vapor diffusion method at 4ºC with commercially available screening kits. If needed, initial hits were optimized by the hanging vapor diffusion method. Final conditions for crystal formation and cryo solutions are listed below, all

grown at 4°C. The peptide-to-protein ratio was kept at 3:1 throughout the co-crystallization attempts. ATP-bound crystal structures were obtained by adding 0.2 µL of reservoir solution containing 10 mM ATP/40 mM $MgCl_2$ to crystal drops. For crystals that had methyl 6-O-(N-heptylcarbamoyl)-α-D-glucopyranoside (hecameg), a detergent in the crystallization condition (a detergent), the crystals were moved to a new drop without Hecameg, and containing 1 mM ATP/4 mM $MgCl_2$. Diffraction data were collected from crystals flash-frozen in liquid nitrogen at a wavelength of 1.5418 Å using a Rigaku MicroMax-007 HF X-ray source, which was coupled to a Rigaku VariMax HF optic system (UMass Amherst). The X-ray data was collected at 100 K.

Crystallization and cryo conditions are listed below:
6X5G: 0.1 M Bicine pH 9, 10% PEG 20K, 2% 1,4-Dioxane (Cryoprotectant: 20% glycerol)
6X5Q: 0.1 M Tris pH 8, 28% PEG 4K (Cryoprotectant: 20% glycerol)
7UIQ: 0.1 M HEPES pH 7, 16% PEG 6K, 0.1% Triton X-114 (Cryoprotectant: 20% ethylene glycol)
7UJQ: 0.1 M Bis-tris methane pH 6.2, 0.1 M ammonium sulfate, 25% PEG 3350, 19mM Hecameg (Cryoprotectant: 20% glycerol)
7UJP: 0.1 M Bis-tris methane pH 6.2, 0.1 M ammonium sulfate, 25% PEG 3350, 19mM Hecameg (Cryoprotectant: 20% glycerol)
7UJR: 0.1 M Bis-tris propane pH 6.2, 0.1 M ammonium sulfate, 20% PEG 3350, 5% ethanol (Cryoprotectant: 20% ethylene glycol)
7UJS: 0.1 M Bis-tris propane pH 6.6, 0.1 M ammonium sulfate, 20% PEG 3350 (Cryoprotectant: 20% ethylene glycol)
7UIR: 0.1 M HEPES pH 7, 16% PEG 6K, 0.1% Triton X-114 (Cryoprotectant: 20% ethylene glycol)
7UJT: 0.1 M Bis-tris propane pH 6.5, 0.2 M Sodium chloride, 25% PEG 3350 (Cryoprotectant: 20% glycerol)
7KL0: 0.1 M Bis-tris methane pH 6.5, 0.1 M Ammonium sulfate, 20% PEG 6000, 19mM Hecameg (Cryoprotectant: 20% ethylene glycol)
7KL1: 0.1 M Bis-tris methane pH 6.5, 0.1 M Ammonium sulfate, 20% PEG 6000, 19mM Hecameg (Cryoprotectant: 20% ethylene glycol)
7UIS: 0.1 M Bis-tris propane pH 6.5, 0.2 M Sodium chloride, 25% PEG 3350 (Cryoprotectant: 20% glycerol)

Data Processing and Structure Determination

Data sets were integrated, merged, and scaled using HKL-2000. The structures were solved by molecular replacement (MR) with Phaser using the coordinates of CaMKIIα kinase domain (PDB ID: 6VZK, 100% amino acid sequence identity) as a search model [48]. Peptides were built into electron density using Coot and refinement was performed with REFMAC5 [49, 50].

Isothermal titration calorimetry

ITC data were obtained using a MicroCal PEAQ-ITC automated calorimeter (Malvern Panalytical, Westborough, MA). Before each titration, interaction partners were dissolved in gel filtration buffer and final buffer conditions of CaMKII kinase domain and interaction partners were matched. GluN2B peptides and CaMKIIN protein contain a single tyrosine residue, which enabled accurate concentration determination. The other peptides lack aromatic residues, and these required crude weight to estimate concentration. Titrations were performed with different peptides as titrant into the cell containing D135N or other mutant CaMKII kinase domains (concentrations are indicated in Table 3). All titrations were performed using the standard 19 injection method, modified to run at 20 °C. The standard 19 injection method in the PEAQ ITC automated control software (v1.40) is one injection of 0.4 µL followed by 18 2 µL injections with a spacing between injections of 150s, a stir speed of 750 rpm, and the reference power set to

558 10. Data were analyzed using PEAQ ITC analysis software (v1.40) using the one-site fitting
559 model, and to eliminate integration of some baseline noise, some integration markers were set
560 manually to obtain better fit.
561
562 **Fluorescence polarization assay**
563 The competition assay was conducted at 1 μM of CaMKII kinase domain (25 mM Tris pH 7.5,
564 150 mM KCl, 1 mM TCEP, 10% glycerol) with 60 nM fluorescein-labeled GluN2B peptide
565 (dissolved in 25 mM Tris pH 7.5, 150 mM KCl, 0.02% Tween, 0.02% Triton) and then titrated
566 increasing concentrations of unlabeled peptide (25 mM Tris pH 7.5, 150 mM KCl, 1 mM TCEP,
567 10% glycerol) at varying concentrations in Corning low volume 384-well black flat bottom plates.
568 The final volume in each well was 20 μL. The fluorescence polarization was measured using a
569 Synergy H1 hybrid plate reader (Biotek) with a filter of 485/20 nm excitation and 528/20 nm
570 emission. Data were fit using a one-site binding equation in GraphPad PRISM version 6.0.
571
572 **Differential scanning calorimetry**
573 All protein samples were diluted to 0.5 mg/mL in DSC buffer (25 mM Tris pH 8,150 mM KCl, 1
574 mM TCEP, 10% glycerol). DSC measurements were performed on a MicroCal Automated
575 PEAQ-DSC instrument (Malvern Panalytical, Westborough, MA). Unless otherwise indicated,
576 after a 5 min pre-scan equilibration step, samples were scanned from 10-120°C at a scan rate
577 of 90°C/hr with no feedback. Data were analyzed using MicroCal PEAQ-DSC software, and
578 baseline-subtracted data were fit to a non-two-state fitting model to obtain apparent T_m values.
579
580 **Molecular Dynamics simulations**
581 Trajectories were run for 1.2 μs - 3.7 μs aggregate time for each complex. All simulations are
582 available for download from Mendeley: DOI: 10.17632/9m3bg3h5rs.1. Starting conformations
583 were taken from co-crystal structures of CaMKIIα kinase domain in complex with peptides
584 derived from GluN2B (PDB:7UJP) and Tiam1 (PDB:7UIR). The sequences used for interaction
585 partners in the simulations are as follows: Tiam1 (1513-1581, adding 28 N-terminal residues
586 and 22 C-terminal residues) as well as GluN2B (1263-1328, adding 32 N-terminal residues and
587 20 C-terminal residues), and the full-length CaMKIIN protein (adding 41 N-terminal residues and
588 22 C-terminal residues). For CaMKIIN, Coot [50] was used to superimpose the structure of a
589 peptide derived from rat CaMKIIN in complex with the kinase domain from *C. elegans* CaMKII
590 (PDB:3KL8) with the structure of GluN2B in complex with the kinase domain of CaMKIIα bound
591 to a Mg^{2+} ion and an ATP molecule (PDB:7UJP). The CaMKIIN peptide and the CaMKIIα kinase
592 domain were then merged into a single structure. Crystallographically unresolved atoms were
593 added, peptides were extended in both N-terminal and C-terminal directions using PDBFixer,
594 part of the OpenMM package [51].
595
596 All simulations were performed with Gromacs 2020.2 [52, 53] and the CHARMM36m force field
597 [53]. Protein complexes were solvated with TIP3P water [54] in dodecahedral boxes that
598 extended 1 nm past the protein in all dimensions. Na^+ ions were added in sufficient quantity to
599 charge neutralize each system. Systems were energy-minimized by steepest descent for 50,000
600 steps using a 0.01 nm step size until the maximum force exerted on any atom fell below 1000
601 kJ/mol/nm. Solvent was equilibrated for 1 ns at constant temperature and volume (NVT
602 ensemble) and another 2 ns at constant temperature and pressure (NPT ensemble) with a
603 positional restraint applied to protein heavy atoms. An additional 10 ns of unrestrained dynamics
604 were simulated prior to collection of production data in order to allow the polypeptide chains to
605 relax from their crystallographic conformations, and allow the simulated systems to equilibrate
606 fully. Periodic boundary conditions were used in all dimensions, bonds were constrained with
607 the LINCS algorithm [55], virtual sites (v-sites) were used to remove the fastest degrees of

608 freedom to facilitate a 4 fs time step [56], particle mesh Ewald (PME) was used to treat
609 electrostatic interactions [57], the v-rescale thermostat [58] with a 0.1 ps coupling time constant
610 was used to maintain the temperature at 300 K, and a cut-off distance of 1.2 nm for neighbor
611 list, Coulomb interactions, and Van der Waals interactions was used throughout system
612 preparation and production simulations. The Parrinello–Rahman barostat [59] with a 2 ps
613 coupling time constant was used to maintain a pressure of 1 bar during NPT equilibration and
614 production simulations. V-site parameters for ATP were determined using MkVsites [60]. GPU-
615 accelerated simulations were performed on two hardware architectures: 1) 2x Intel Xeon Silver
616 4110 cpu (8 Cores), 2x nVidia Tesla V100 gpu; 2) 2x Intel Xeon Gold 6140 cpu (18 Cores), 2x
617 nVidia Tesla V100 gpu. In order to obtain comparable aggregate lengths of production
618 simulations for the three simulated systems, two independent simulations of the
619 kinase:CaMKIIN complex were carried out.
620
621 To calculate RMSD and RMSF during the simulations, trajectories were aligned about the Cα of
622 the kinase domain. RMSD was calculated with VMD [61]. RMSF was calculated with ProDy [62]
623 as interfaced with VMD. RMSD and RMSF of the peptide were calculated with the kinases
624 aligned to determine how the residues of the peptide fluctuated with respect to the kinase.
625
626 One production simulation was performed for each of the wild type kinase:GluN2B and wild type
627 kinase:Tiam1 complexes, producing trajectories of 2.19 μs and 2.05 μs, respectively. Two
628 independent simulations were performed for the wild type kinase:CaMKIIN. The CaMKIIN
629 trajectories were 0.46 μs and 1.84 μs in length, for an aggregate of 2.3 μs. The GluN2B
630 trajectories were 0.68 μs and 0.57 μs in length, for an aggregate of 1.25 μs. Trajectories were
631 analyzed using MDTraj [63]. Hydrophobic contact distance between two residues was defined
632 as the shortest distance between side chain heavy atoms. Pairwise RMSD between frames for
633 specific hydrophobic interactions (kinase residues F98, I101, V102, I205, and peptide residue in
634 -5 position adjusted from sequence alignment; kinase residue W214, Ile at –5, Pro at –10 in
635 CaMKIIN peptide, see Fig 2B) was calculated based on side chain heavy atoms for the residues
636 involved in the interaction: 5 residues for the first interaction, 3 residues for the second.
637
638 **Coupled kinase assays**
639 Kinase activity was monitored using a Synergy H1 microplate reader (Biotek) as previously
640 described [22, 64]. The assay was conducted in 50 mM Tris, 150 mM KCl, 10 mM $MgCl_2$, 2 mM
641 ATP, 1 mM Phosphoenolpyruvate (Alfa Aesar), 0.2 mM Nicotinamide adenine dinucleotide
642 (Sigma), 10 units/mL Pyruvate kinase (Sigma), 30 units/mL Lactate dehydrogenase (Millipore
643 Sigma), varying concentrations of Syntide-2 (Lifetein). The final CaMKII kinase domain
644 concentration was 5 nM. 500 nM CaMKIIN protein or 8.14 μM NMDAR(S1303D) peptide was
645 preincubated with CaMKII kinase domain before adding to the reaction mix of corresponding
646 experiments. The reactions were started by the addition of ATP to the reaction mix and the
647 absorbance was measured at 340 nM at 30°C at 10 and 15 sec intervals for 10 minutes. The
648 rate was obtained by calculating the maximum observed slope of each reaction. Data were fit
649 using the Michaelis-Menten equation in GraphPad PRISM version 6.01.
650
651 **Immunoprecipitation**
652 HEK293T cell lysates were prepared in lysis buffer (50 mM Tris-HCl pH 7.5, 150 mM NaCl, 1%
653 Triton X-100, 10% glycerol, 1 mM Na_3VO_4, 10 mM NaF, 1 mM β-glycerophosphate, 1 x
654 phosphatase inhibitor cocktail (Nacalai, Kyoto, Japan), 1x cOmplete tablet (Roche, Basel,
655 Switzerland) and centrifuged at 14,000 rpm for 10 min at 4°C. The supernatant was subjected to
656 immunoprecipitation using 20 μL of the anti-Flag antibody-beads (Sigma) for 2-4 hours at 4°C.

657 Beads were washed with 1 mL of lysis buffer for three times. Bound proteins were eluted with
658 SDS-PAGE sample buffer and subjected to western blotting.
659
660 **Data availability**
661 Atomic structures have been deposited in the PDB, listed in the table below.
662
663 Table of PDB codes and descriptions.
664

6X5G	D135N kinase in complex with densin-180
6X5Q	D135N kinase in complex with GluA1
7UIQ	D135N kinase in complex with Tiam1
7UIR	D135N kinase in complex with Tiam1 and ATP
7UJQ	D135N kinase in complex with GluN2B and Hecameg
7UJP	D135N kinase in complex with GluN2B and ATP
7UJR	WT kinase in complex with GluN2B
7UJS	WT kinase in complex with GluN2B and ADP
7KL0	D135N kinase in complex with phosphomimetic GluN2B and Hecameg
7KL1	D135N kinase in complex with phosphomimetic GluN2B and ATP
7UIS	D135N kinase in complex with phosphomimetic GluN2B
7UJT	D135N kinase in complex with phosphomimetic GluN2B and ATP

665

666 **ACKNOWLEDGMENTS**

667 We thank Roger Colbran, Howard Schulman, Eric Strieter and Peter Chien for helpful
668 discussions. We thank Josh Pajak for help with MD simulations. This work was supported by
669 funds from NIGMS R01123157 (M.S.), SPIRITS 2019 of Kyoto University, Grant-in-Aid for
670 Scientific Research JP18H04733, and JP18H05434 from the MEXT, CREST JPMJCR20E4
671 from JST, Japan and HFSP Research Grant (RGP0020/2019) (Y.H.).

672
673 Conflict of interest: YH received research funds from Fujitsu Laboratories and Dwango.

674 **Author Contributions**
675 C.Ö. solved all crystal structures and performed all FP measurements and kinetic assays. T.M.
676 and T.S. performed immunoprecipitation experiments. N.S., E.A., C.G., E.L., J.F. and E.A.E.
677 also assisted with experiments under supervision of B.A.K., S.C.G., Y.H. and M.M.S. R.S.
678 performed molecular dynamics. C.Ö., R.S., Y.H., B.A.K., and M.M.S. wrote and edited the
679 manuscript.
680
681 **REFERENCES**
682

683 1. Lisman, J., R. Yasuda, and S. Raghavachari, *Mechanisms of CaMKII action in long-term*
684 *potentiation.* Nat Rev Neurosci, 2012. **13**(3): p. 169-82.
685 2. Malenka, R.C., et al., *An essential role for postsynaptic calmodulin and protein kinase*
686 *activity in long-term potentiation.* Nature, 1989. **340**(6234): p. 554-7.
687 3. Sloutsky, R. and M.M. Stratton, *Functional implications of CaMKII alternative splicing.*
688 Eur J Neurosci, 2020.

689 4. Erondu, N.E. and M.B. Kennedy, *Regional distribution of type II Ca^{2+}/calmodulin-*
690 *dependent protein kinase in rat brain.* J Neurosci, 1985. **5**(12): p. 3270-7.
691 5. Lynch, M.A., *Long-term potentiation and memory.* Physiol Rev, 2004. **84**(1): p. 87-136.
692 6. Ishida, A. and H. Fujisawa, *Stabilization of Calmodulin-Dependent Protein-Kinase-Ii*
693 *through the Autoinhibitory Domain.* Journal of Biological Chemistry, 1995. **270**(5): p.
694 2163-2170.
695 7. Bayer, K.U., et al., *Interaction with the NMDA receptor locks CaMKII in an active*
696 *conformation.* Nature, 2001. **411**(6839): p. 801-5.
697 8. Bayer, K.U., et al., *Transition from reversible to persistent binding of CaMKII to*
698 *postsynaptic sites and NR2B.* J Neurosci, 2006. **26**(4): p. 1164-74.
699 9. Saneyoshi, T., et al., *Reciprocal Activation within a Kinase-Effector Complex Underlying*
700 *Persistence of Structural LTP.* Neuron, 2019. **102**(6): p. 1199-1210 e6.
701 10. Sun, X.X., et al., *The eag potassium channel binds and locally activates*
702 *calcium/calmodulin-dependent protein kinase II.* J Biol Chem, 2004. **279**(11): p. 10206-
703 14.
704 11. Strack, S. and R.J. Colbran, *Autophosphorylation-dependent targeting of calcium/*
705 *calmodulin-dependent protein kinase II by the NR2B subunit of the N-methyl- D-*
706 *aspartate receptor.* J Biol Chem, 1998. **273**(33): p. 20689-92.
707 12. Strack, S., R.B. McNeill, and R.J. Colbran, *Mechanism and regulation of*
708 *calcium/calmodulin-dependent protein kinase II targeting to the NR2B subunit of the N-*
709 *methyl-D-aspartate receptor.* J Biol Chem, 2000. **275**(31): p. 23798-806.
710 13. Omkumar, R.V., et al., *Identification of a phosphorylation site for*
711 *calcium/calmodulindependent protein kinase II in the NR2B subunit of the N-methyl-D-*
712 *aspartate receptor.* J Biol Chem, 1996. **271**(49): p. 31670-8.
713 14. Castro-Rodrigues, A.F., et al., *The Interaction between the Drosophila EAG Potassium*
714 *Channel and the Protein Kinase CaMKII Involves an Extensive Interface at the Active Site*
715 *of the Kinase.* J Mol Biol, 2018. **430**(24): p. 5029-5049.
716 15. Walikonis, R.S., et al., *Densin-180 forms a ternary complex with the (α)-subunit of*
717 *Ca^{2+}/calmodulin-dependent protein kinase II and (α)-actinin.* J Neurosci, 2001. **21**(2): p.
718 423-33.
719 16. Jiao, Y., et al., *Characterization of a central Ca^{2+}/calmodulin-dependent protein kinase*
720 *IIα/β binding domain in densin that selectively modulates glutamate receptor subunit*
721 *phosphorylation.* J Biol Chem, 2011. **286**(28): p. 24806-18.
722 17. Mammen, A.L., et al., *Phosphorylation of the α-amino-3-hydroxy-5-methylisoxazole4-*
723 *propionic acid receptor GluR1 subunit by calcium/calmodulin-dependent kinase II.* J Biol
724 Chem, 1997. **272**(51): p. 32528-33.
725 18. Barria, A., V. Derkach, and T. Soderling, *Identification of the Ca^{2+}/calmodulin-dependent*
726 *protein kinase II regulatory phosphorylation site in the α-amino-3-hydroxyl-5-methyl-4-*
727 *isoxazole-propionate-type glutamate receptor.* J Biol Chem, 1997. **272**(52): p. 32727-30.
728 19. Diering, G.H. and R.L. Huganir, *The AMPA Receptor Code of Synaptic Plasticity.* Neuron,
729 2018. **100**(2): p. 314-329.
730 20. Barria, A., et al., *Regulatory phosphorylation of AMPA-type glutamate receptors by CaM-*
731 *KII during long-term potentiation.* Science, 1997. **276**(5321): p. 2042-5.

732 21. Derkach, V., A. Barria, and T.R. Soderling, *Ca^{2+}/calmodulin-kinase II enhances channel*
733 *conductance of α-amino-3-hydroxy-5-methyl-4-isoxazolepropionate type glutamate*
734 *receptors.* Proc Natl Acad Sci U S A, 1999. **96**(6): p. 3269-74.
735 22. Chao, L.H., et al., *Intersubunit capture of regulatory segments is a component of*
736 *cooperative CaMKII activation.* Nat Struct Mol Biol, 2010. **17**(3): p. 264-72.
737 23. Wang, C., et al., *A novel endogenous human CaMKII inhibitory protein suppresses tumor*
738 *growth by inducing cell cycle arrest via p27 stabilization.* J Biol Chem, 2008. **283**(17): p.
739 11565-74.
740 24. Zhang, J., et al., *Molecular cloning and characterization of a novel calcium/calmodulin-*
741 *dependent protein kinase II inhibitor from human dendritic cells.* Biochem Biophys Res
742 Commun, 2001. **285**(2): p. 229-34.
743 25. Chang, B.H., S. Mukherji, and T.R. Soderling, *Calcium/calmodulin-dependent protein*
744 *kinase II inhibitor protein: localization of isoforms in rat brain.* Neuroscience, 2001.
745 **102**(4): p. 767-77.
746 26. White, R.R., et al., *Definition of optimal substrate recognition motifs of Ca^{2+}-calmodulin-*
747 *dependent protein kinases IV and II reveals shared and distinctive features.* J Biol Chem,
748 1998. **273**(6): p. 3166-72.
749 27. Songyang, Z., et al., *A structural basis for substrate specificities of protein Ser/Thr*
750 *kinases: primary sequence preference of casein kinases I and II, NIMA, phosphorylase*
751 *kinase, calmodulin-dependent kinase II, CDK5, and Erk1.* Mol Cell Biol, 1996. **16**(11): p.
752 6486-93.
753 28. Ishida, A., et al., *Critical amino acid residues of AIP, a highly specific inhibitory peptide of*
754 *calmodulin-dependent protein kinase II.* FEBS Lett, 1998. **427**(1): p. 115-8.
755 29. Stokoe, D., et al., *The substrate specificity and structure of mitogen-activated protein*
756 *(MAP) kinase-activated protein kinase-2.* Biochem J, 1993. **296 (Pt 3)**: p. 843-9.
757 30. Coultrap, S.J. and K.U. Bayer, *Improving a natural CaMKII inhibitor by random and*
758 *rational design.* PLoS One, 2011. **6**(10): p. e25245.
759 31. Rust, H.L. and P.R. Thompson, *Kinase consensus sequences: a breeding ground for*
760 *crosstalk.* ACS Chem Biol, 2011. **6**(9): p. 881-92.
761 32. Yang, E. and H. Schulman, *Structural examination of autoregulation of multifunctional*
762 *calcium/calmodulin-dependent protein kinase II.* J Biol Chem, 1999. **274**(37): p. 26199-
763 208.
764 33. Rellos, P., et al., *Structure of the CaMKIIδ/calmodulin complex reveals the molecular*
765 *mechanism of CaMKII kinase activation.* PLoS Biol, 2010. **8**(7): p. e1000426.
766 34. Vulpetti, A. and R. Bosotti, *Sequence and structural analysis of kinase ATP pocket*
767 *residues.* Farmaco, 2004. **59**(10): p. 759-65.
768 35. Zha, M., et al., *Crystal structures of human CaMKIα reveal insights into the regulation*
769 *mechanism of CaMKI.* PLoS One, 2012. **7**(9): p. e44828.
770 36. Rosenberg, O.S., et al., *Structure of the autoinhibited kinase domain of CaMKII and SAXS*
771 *analysis of the holoenzyme.* Cell, 2005. **123**(5): p. 849-60.
772 37. Nolen, B., S. Taylor, and G. Ghosh, *Regulation of protein kinases; controlling activity*
773 *through activation segment conformation.* Mol Cell, 2004. **15**(5): p. 661-75.
774 38. Pellicena, P. and H. Schulman, *CaMKII inhibitors: from research tools to therapeutic*
775 *agents.* Front Pharmacol, 2014. **5**: p. 21.

776 39. Torres-Ocampo, A.P., et al., *Characterization of CaMKIIα holoenzyme stability.* Protein
777 Science, 2020. **29**: p. 1524-1534.
778 40. Hornbeck, P.V., et al., *PhosphoSitePlus, 2014: mutations, PTMs and recalibrations.*
779 Nucleic Acids Res, 2015. **43**(Database issue): p. D512-20.
780 41. McCoy, F., et al., *Metabolic activation of CaMKII by coenzyme A.* Mol Cell, 2013. **52**(3): p.
781 325-39.
782 42. Kennelly, P.J. and E.G. Krebs, *Consensus sequences as substrate specificity determinants*
783 *for protein kinases and protein phosphatases.* J Biol Chem, 1991. **266**(24): p. 15555-8.
784 43. Pearson, R.B. and B.E. Kemp, *Protein kinase phosphorylation site sequences and*
785 *consensus specificity motifs: tabulations.* Methods Enzymol, 1991. **200**: p. 62-81.
786 44. Endicott, J.A., M.E. Noble, and L.N. Johnson, *The structural basis for control of eukaryotic*
787 *protein kinases.* Annu Rev Biochem, 2012. **81**: p. 587-613.
788 45. Mao, L.M., et al., *Phosphorylation and regulation of glutamate receptors by CaMKII.*
789 Sheng Li Xue Bao, 2014. **66**(3): p. 365-72.
790 46. Hosokawa, T., et al., *Stoichiometry and phosphoisotypes of hippocampal AMPA-type*
791 *glutamate receptor phosphorylation.* Neuron, 2015. **85**(1): p. 60-67.
792 47. Schulman, H., *Activity-dependent regulation of calcium/calmodulin-dependent protein*
793 *kinase II localization.* J Neurosci, 2004. **24**(39): p. 8399-403.
794 48. McCoy, A.J., et al., *Phaser crystallographic software.* J Appl Crystallogr, 2007. **40**(Pt 4): p.
795 658-674.
796 49. Murshudov, G.N., A.A. Vagin, and E.J. Dodson, *Refinement of macromolecular structures*
797 *by the maximum-likelihood method.* Acta Crystallogr D Biol Crystallogr, 1997. **53**(Pt 3): p.
798 240-55.
799 50. Winn, M.D., et al., *Overview of the CCP4 suite and current developments.* Acta
800 Crystallogr D Biol Crystallogr, 2011. **67**(Pt 4): p. 235-42.
801 51. Eastman, P., et al., *OpenMM 4: A Reusable, Extensible, Hardware Independent Library*
802 *for High Performance Molecular Simulation.* J Chem Theory Comput, 2013. **9**(1): p. 461-
803 469.
804 52. Pall, S., et al., *Tackling Exascale Software Challenges in Molecular Dynamics Simulations*
805 *with GROMACS.* Solving Software Challenges for Exascale, 2015. **8759**: p. 3-27.
806 53. Huang, J., et al., *CHARMM36m: an improved force field for folded and intrinsically*
807 *disordered proteins.* Nat Methods, 2017. **14**(1): p. 71-73.
808 54. Jorgensen, W.L., et al., *Comparison of Simple Potential Functions for Simulating Liquid*
809 *Water.* Journal of Chemical Physics, 1983. **79**(2): p. 926-935.
810 55. Hess, B., *P-LINCS: A Parallel Linear Constraint Solver for Molecular Simulation.* J Chem
811 Theory Comput, 2008. **4**(1): p. 116-22.
812 56. Feenstra, K.A., B. Hess, and H.J.C. Berendsen, *Improving efficiency of large time-scale*
813 *molecular dynamics simulations of hydrogen-rich systems.* Journal of Computational
814 Chemistry, 1999. **20**(8): p. 786-798.
815 57. Essmann, U., et al., *A Smooth Particle Mesh Ewald Method.* Journal of Chemical Physics,
816 1995. **103**(19): p. 8577-8593.
817 58. Bussi, G., D. Donadio, and M. Parrinello, *Canonical sampling through velocity rescaling.* J
818 Chem Phys, 2007. **126**(1): p. 014101.

59. Parrinello, M. and A. Rahman, *Polymorphic Transitions in Single-Crystals - a New Molecular-Dynamics Method.* Journal of Applied Physics, 1981. **52**(12): p. 7182-7190.
60. Larsson, P., R.C. Kneiszl, and E.G. Marklund, *MkVsites: A tool for creating GROMACS virtual sites parameters to increase performance in all-atom molecular dynamics simulations.* J Comput Chem, 2020. **41**(16): p. 1564-1569.
61. Humphrey, W., A. Dalke, and K. Schulten, *VMD: visual molecular dynamics.* J Mol Graph, 1996. **14**(1): p. 33-8, 27-8.
62. Bakan, A., L.M. Meireles, and I. Bahar, *ProDy: protein dynamics inferred from theory and experiments.* Bioinformatics, 2011. **27**(11): p. 1575-7.
63. McGibbon, R.T., et al., *MDTraj: A Modern Open Library for the Analysis of Molecular Dynamics Trajectories.* Biophys J, 2015. **109**(8): p. 1528-32.
64. Barker, S.C., et al., *Characterization of pp60c-src tyrosine kinase activities using a continuous assay: autoactivation of the enzyme is an intermolecular autophosphorylation process.* Biochemistry, 1995. **34**(45): p. 14843-51.

FIGURES

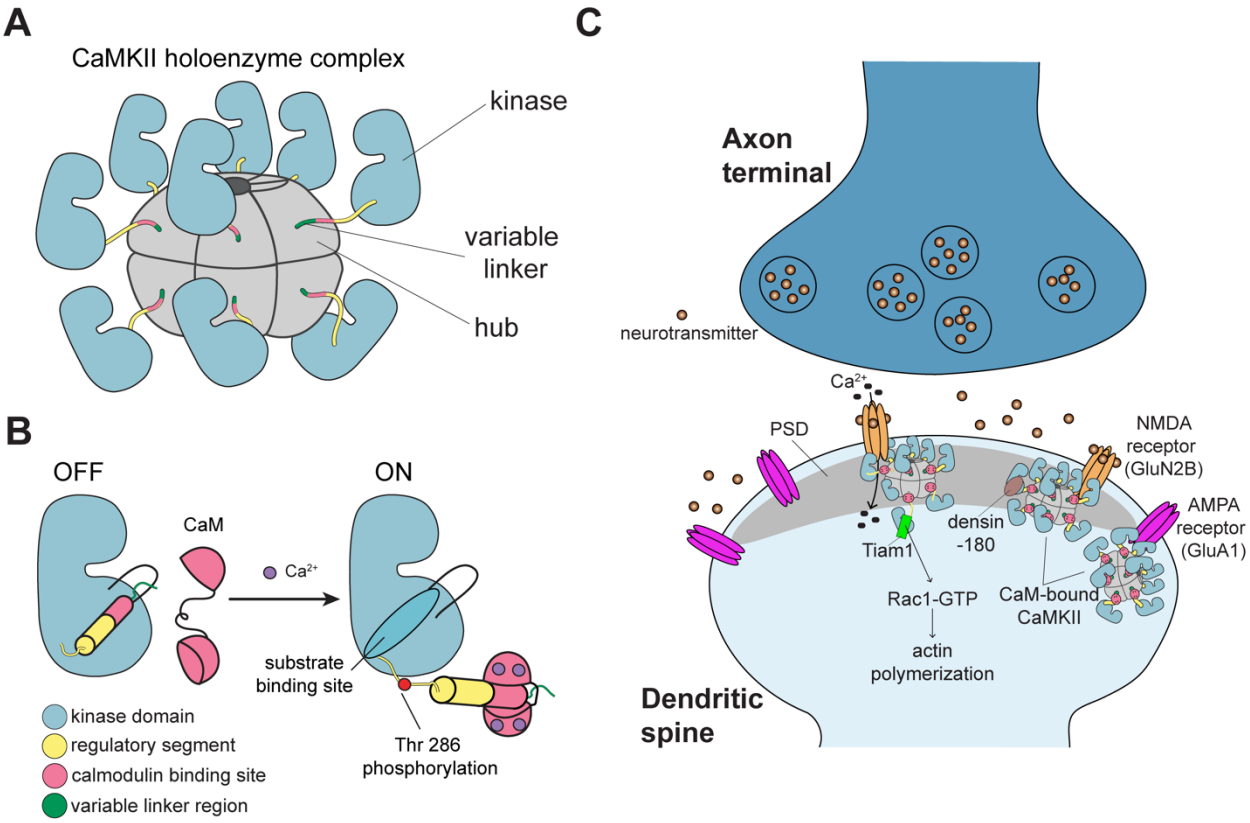

Figure 1. CaMKII architecture and the interaction partners at excitatory synapses
(A) The architecture of a dodecameric CaMKII holoenzyme. (B) Ca^{2+}/CaM binding activates CaMKII by competitively binding the regulatory segment thereby freeing the substrate binding site. Active CaMKII autophosphorylates at Thr 286. (C) CaMKII interactions at the excitatory postsynaptic structure, mostly in the post synaptic density (PSD), of the dendritic spine.

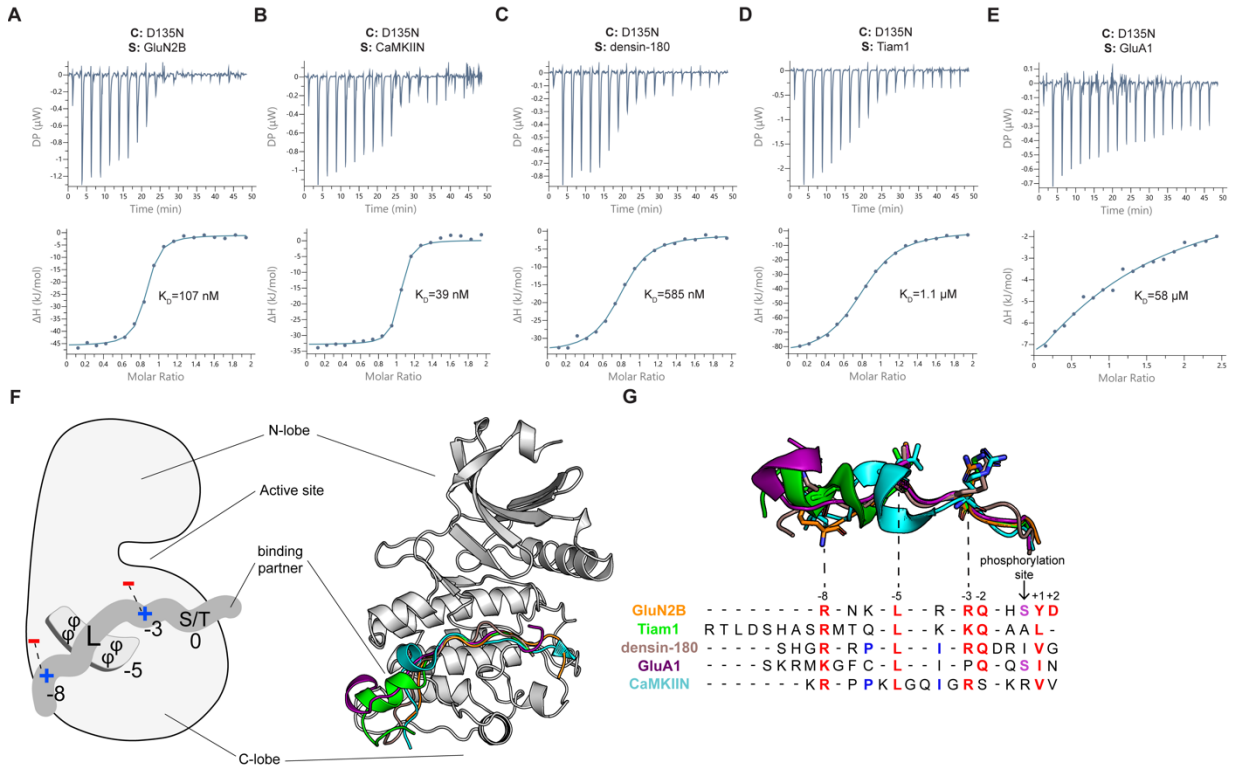

Figure 2. There is a single binding site on the CaMKII kinase domain. (A-E) Representative ITC measurements of D135N kinase domain binding to peptide partners. Contents of the cell (C) and syringe (S) used are listed in the figure panels. The mean K_d value from two independent measurements is labeled in the figure. (F) Left: Schematic diagram of the interactions with binding partners. Phi symbol indicates hydrophobic residues. Right: overlay of five cocrystal structures, peptides shown as cartoon in corresponding colors seen in key to the right. (G) The sequence alignment of CaMKII binding partners. Binding partner position numbering is based on the prototypical GluN2B substrate with the phosphorylation site set to zero. Aligned peptide structures are above for reference. Conserved residues are colored red. Phosphorylatable residues at the phosphorylation site are colored purple. Residues involved in a docking event with W214 are colored blue.

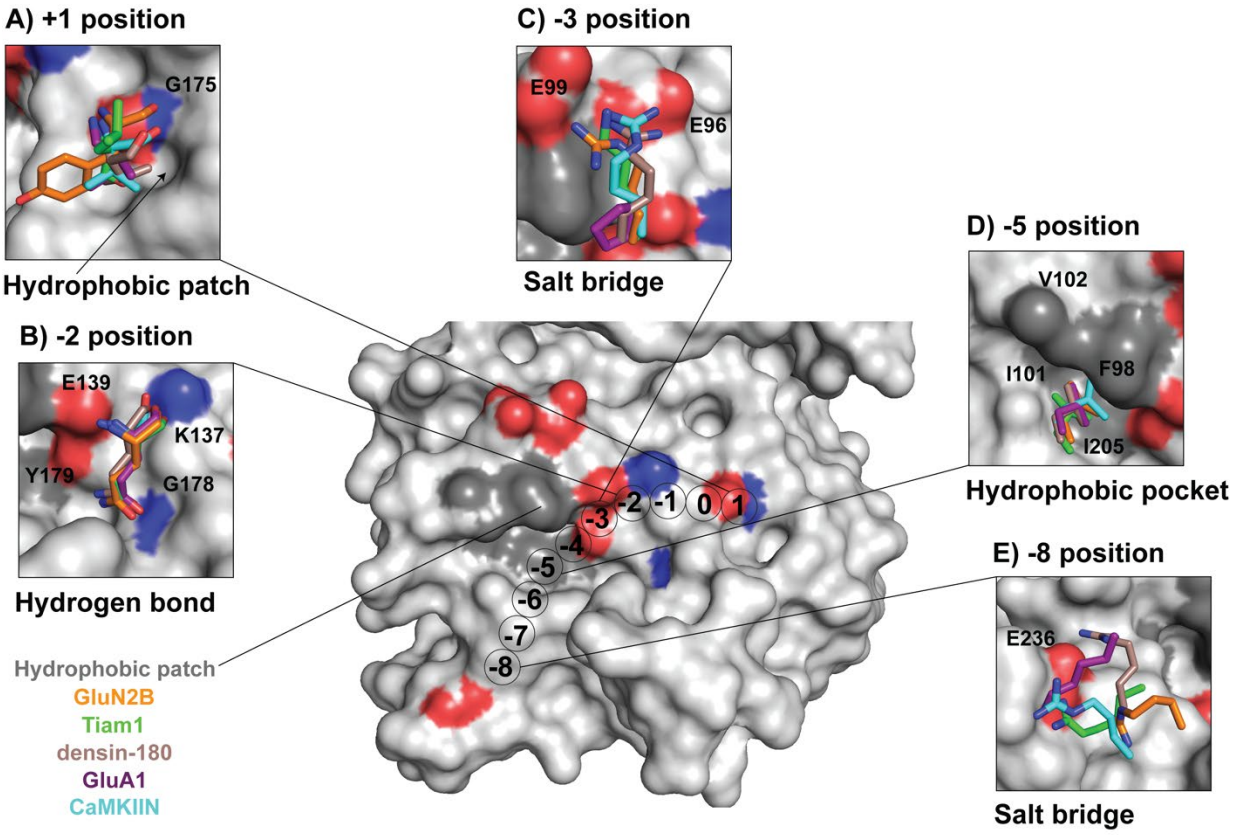

Figure 3. Conserved binding motifs on the catalytic domain surface.
Surface representation of the CaMKII kinase domain highlighting residues that mediate interactions with binding partners. Color code matches previous figures (GluN2B: orange, Tiam1: green, densin-180: brown, GluA1: purple, CaMKIIN: cyan). (A) At the +1 position, a hydrophobic patch (arrow) is formed by F173, P177, L185, and Y222. GluA1, CaMKIIN, and densin-180 all have Val or Ile at the +1 position, which are buried in this hydrophobic groove. Backbone atoms of the +1 residue hydrogen bond with the backbone of G175 (highlighted red and blue on the structure). (B) At the -2 position, all interactors have a glutamine except for CaMKIIN, which has a serine. The glutamine sidechain amide oxygen forms a hydrogen bond with the backbone of G178, and the amino group interacts with the sidechain of Y179. The backbone carbonyl interacts with sidechain of K137, and the backbone amino group interacts with E139. (C) At the -3 position, lysine or arginine interact with E96 and E99. The basic residues of interaction partners are positioned 2.4 – 4.2 Å between E96 and E99. GluA1 has a proline at the -3 position, which is flipped away from E96/99. (D) At the -5 position, a conserved leucine across all interactors nestles into a hydrophobic pocket formed by F98, I101, V102, and I205. (E) Lysine or arginine at the -8 position forms a salt bridge with E236.

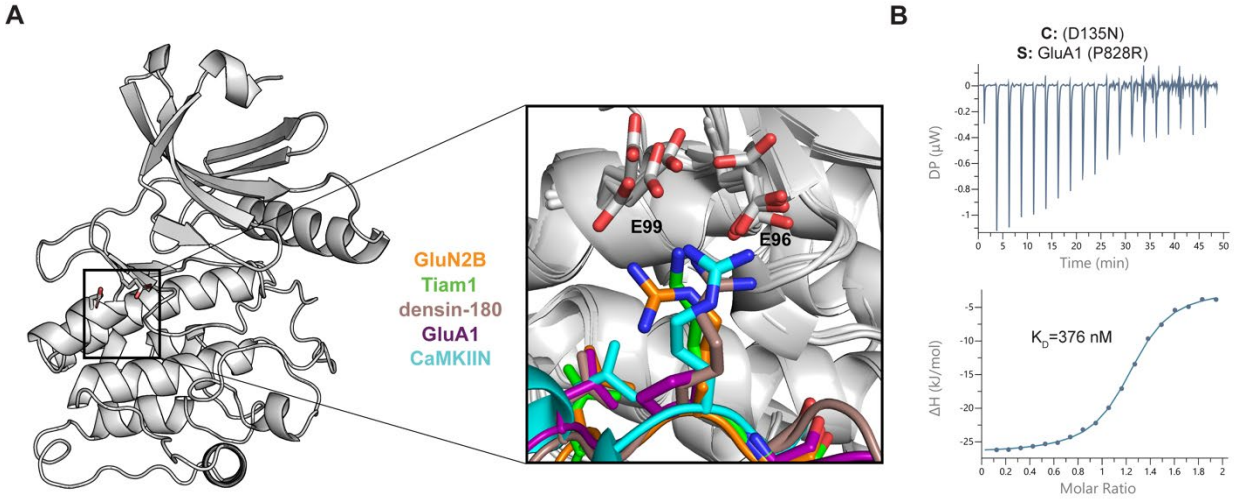

Figure 4. Electrostatic interactions with a basic residue at -3 position facilitate high affinity binding. (A) CaMKII kinase domain shown as a cartoon, E96 and E99 residues are shown as sticks. A zoomed in view of all five co-crystal structures are overlaid to highlight the basic residue at the -3 position (except for GluA1 in purple) interacting with the two glutamic acids in the kinase domain. (B) ITC data between D135N CaMKII kinase domain (cell) and GluA1 with P828R mutation (syringe). The mean K_d value is from two independent measurements.

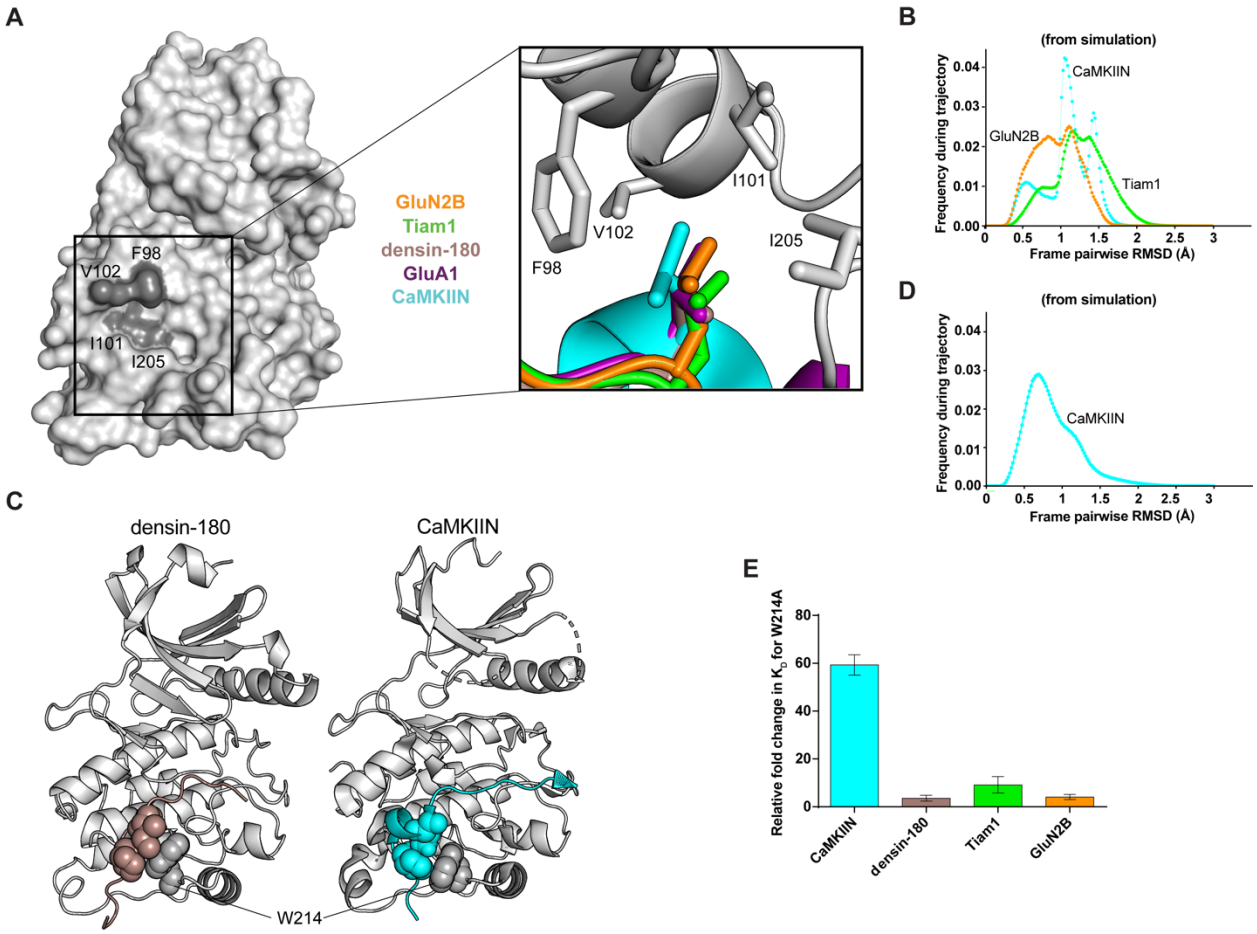

Figure 5. Hydrophobic interactions mediate binding. (A) Surface representation of CaMKII kinase domain with residues forming the hydrophobic pocket labeled (dark gray). Inset: overlay of leucine residues from all co-crystal structures bound in the hydrophobic pocket. (B) Histograms of RMSD from MD simulations between every pair of trajectory frames for F98, I101, V102, and I205 with -5 peptide leucine. (C) Crystal structures with sphere representation of the isoleucine and proline or leucine residue of densin-180 (brown) and CaMKIIN (cyan) docking onto W214 (gray) of kinase domain. (D) RMSD histogram from MD simulations for W214 interacting with isoleucine and proline of CaMKIIN. (E) K_d values were extracted from ITC data and relative fold changes were calculated by dividing the observed K_d from the mutant (W214A) by the D135N kinase domain. Standard deviations from the mean are shown as error bars for duplicate measurements.

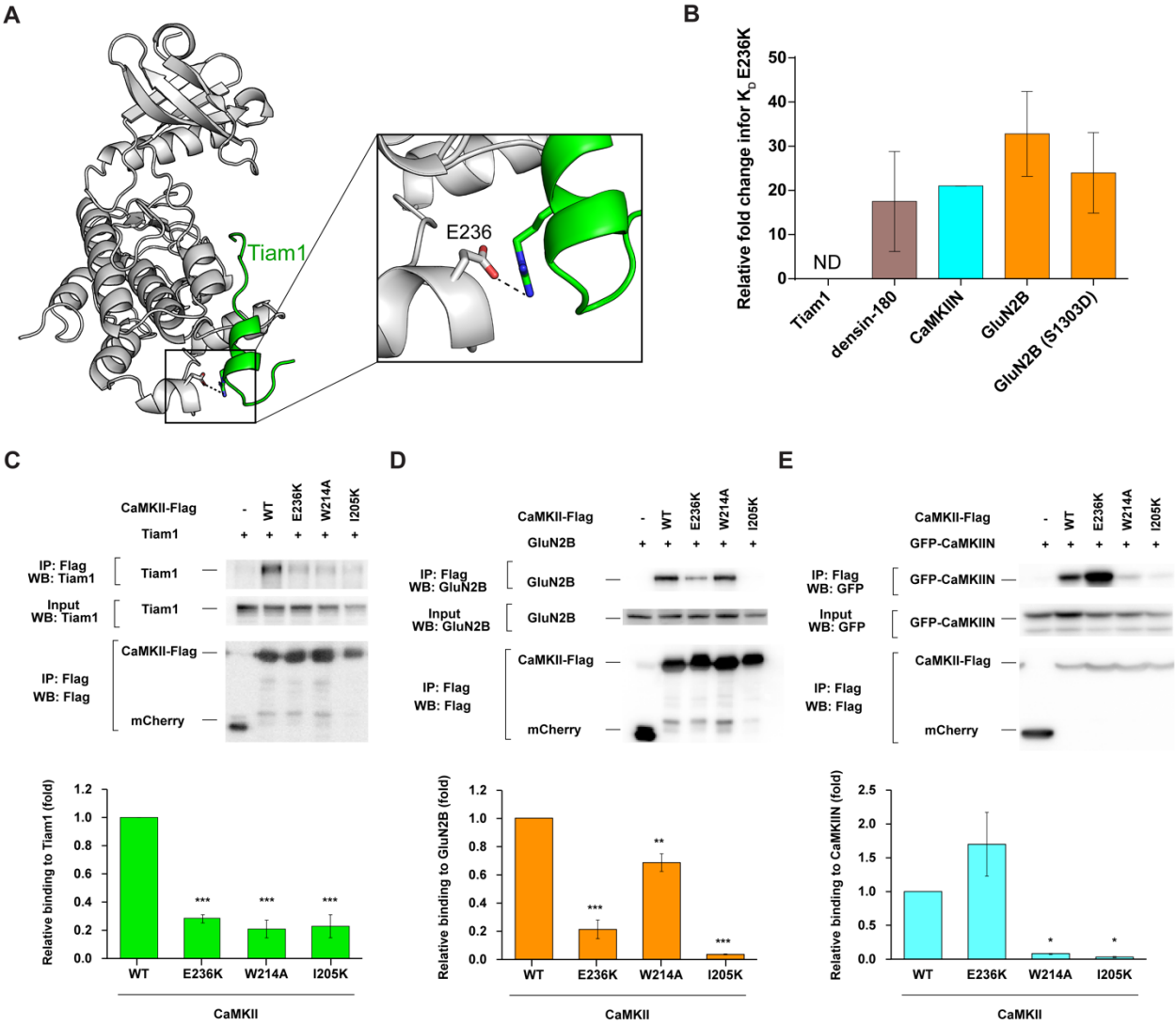

Figure 6. Electrostatic interaction with E236 facilitates binding. (A) View of the interaction between CaMKII E236 (gray) and Tiam1 R1549 (green). (B) K_d values were extracted from ITC data and relative fold changes were calculated by dividing the observed K_d from the mutant (E236K) by the D135N kinase domain. Standard deviations from the mean are shown as error bars for duplicate measurements. (C-E) Effects of CaMKII mutations (E236K, W214A, and

I205K) on interactions with Tiam1, GluN2B, and CaMKIIN. HEK293T cells were co-transfected with Flag-tagged CaMKII variants and Tiam1-mGFP, GluN2B or EGFP-CaMKIIN. Cell lysates were immunoprecipitated with Flag antibody, and samples were immunoblotted with Tiam1, GluN2B, GFP, and Flag antibodies. Representative blots are shown in upper panels. Quantification of the co-immunoprecipitation from 3 or 4 independent experiments were shown in a graph of (C) Tiam1 (n=3) (D) GluN2B (n=3) (E) CaMKIIN (n=4). Error bars indicate standard error of the means. The amount of co-immunoprecipitated Tiam1, GluN2B or CaMKIIN was normalized by the amount in cell lysate and immunoprecipitated CaMKII. *p < 0.05, **, < 0.01 and ***, < 0.001, compared to WT CaMKII; one-way ANOVA with the Shaffer's post hoc test comparisons. WT, wild type; IP, immunoprecipitation.

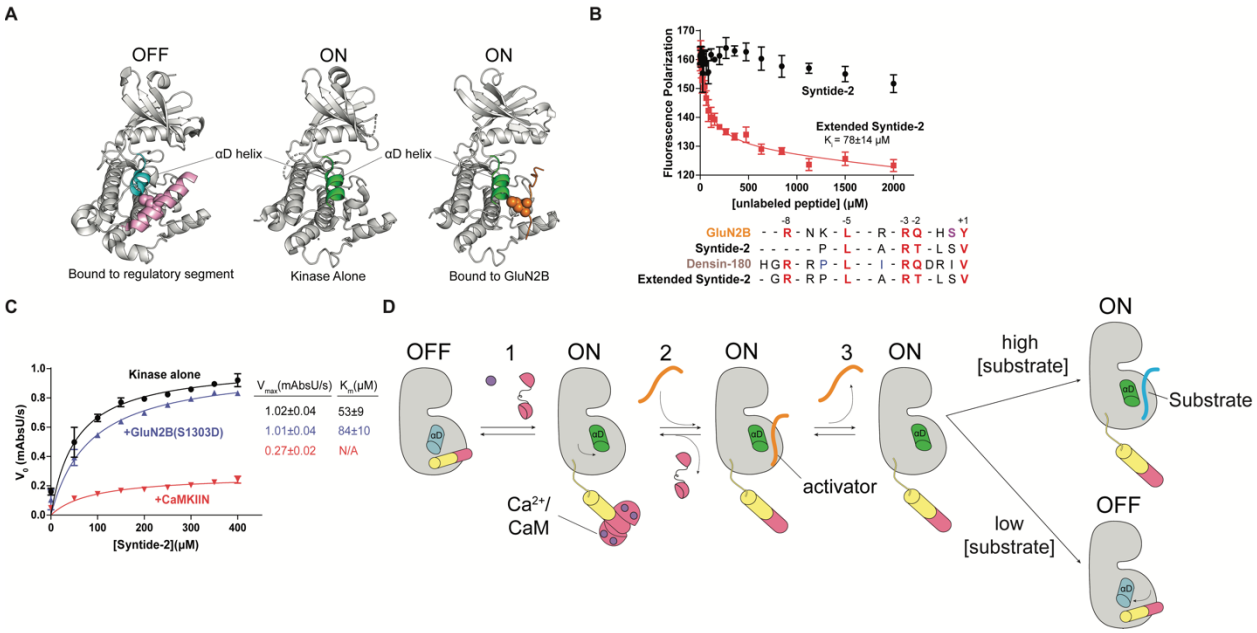

Figure 7. GluN2B acts as a competitive inhibitor on CaMKII

(A) Comparison of the αD helix between crystal structures of the autoinhibited with regulatory segment (pink) bound (left, PDB:2VZ6), uninhibited kinase with no regulatory segment (middle, PDB:6VZK), and active kinase with GluN2B (orange) bound (right, PDB:7UIS). The αD helix goes from rotated inward in the off-state (blue) to rotated outward 45° in the on-state (green). (B) Competition assay against GluN2B using Syntide-2 (black) and extended version of Syntide-2 (red). Sequence alignment of GluN2B, Syntide-2, densin-180, and the extended Syntide-2 is shown below the graph. For clarity, the alignments start at the +1 position (C-terminal end) and contain the -8 basic residue (N-terminal end). Full sequences used are listed in the Methods section. (C) Coupled kinase assay results with kinase alone, in the presence of GluN2B and CaMKIIN. The significance of the change in K_m values is significant using unpaired t test with Welch's correction, p=0.0208. (D) Proposed model of maintaining CaMKII activity by binding to a high affinity activator. CaMKII binds Ca^{2+}/CaM and is activated, and the αD helix rotates out (Rxn 1). A high affinity activator binds to the substrate binding site (Rxn 2). When the Ca^{2+} signal dissipates, CaM dissociates from CaMKII, but the activator remains bound, competing with the regulatory segment. The activator dissociates, but the αD helix remains in the active conformation (Rxn 3). In high [substrate], substrate will bind and be phosphorylated. In low [substrate], either the activator will rebind, or the αD helix will rotate back in to accommodate regulatory segment binding.

SUPPLEMENTAL FIGURES

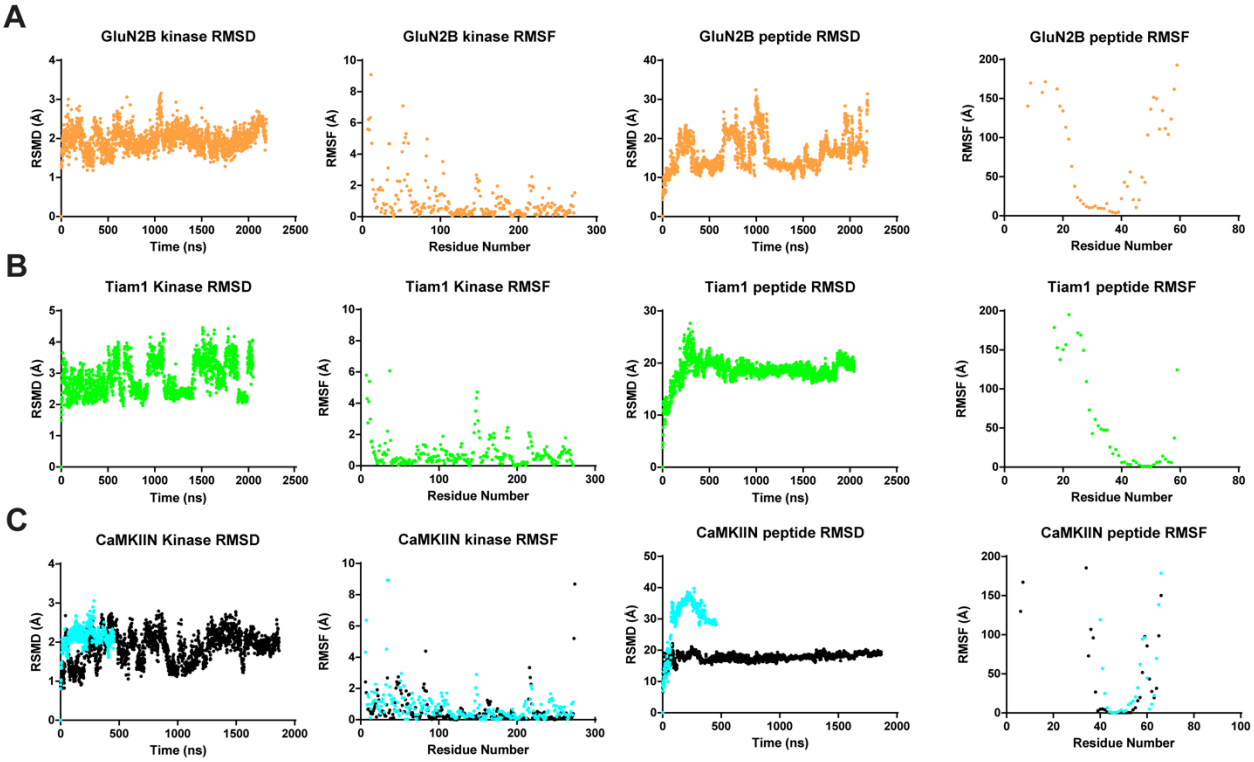

Figure S1. RMSD and RMSF calculations from MD trajectories. RMSD and RMSF were calculated for both the kinase domain and the peptide for each of the trajectories. For CaMKIIN, the two trajectories are overlaid (cyan:0.46 μs and black:1.84 μs). For the kinase domains, RMSD and RMSF values are largely ~3 Å or less, with higher values at the termini, indicating high stability. For the peptides, RMSD values are higher which is not surprising considering this is a largely flexible polypeptide. Peptide RMSF plots are shown up to 200 Å. In the bound regions (residues ~23-40 in GluN2B, ~40-60 in Tiam1 and CaMKIIN) the RMSF values are quite low (<4 Å) indicating high stability. Whereas there is high mobility at the termini.

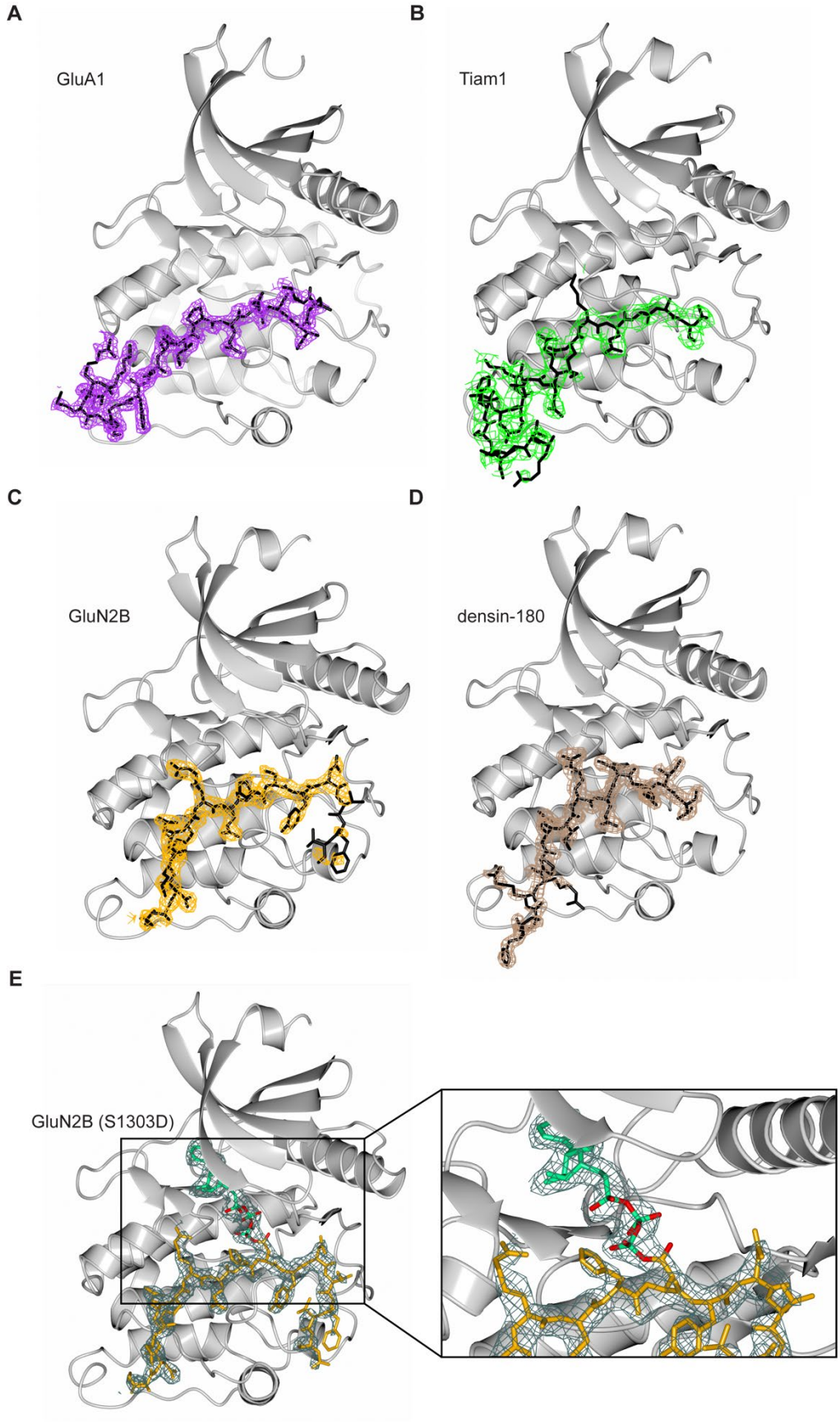
A
GluA1
B
Tiam1
C
GluN2B
D
densin-180
E
GluN2B (S1303D)

Figure S2. Structures of CaMKII kinase domain bound to peptide binding partners. Electron-density omit maps are shown as mesh for all peptide binding partners at σ=1. CaMKII kinase domain shown in light gray (A) GluA1 (PDB:6X5Q) in purple, (B) Tiam1(PDB:7UIQ) in green, (C) GluN2B (PDB:7UJQ) in orange, (D) densin-180 (PDB:6X5G) in brown, and (E) GluN2B (S1303D) in presence of ATP (PDB:7KL1). For (E), the peptide is shown in orange and omit map is shown in dark gray, ATP is colored green. D1303 sidechain is covalently linked to ATP molecule and is shown in red together with the phosphate oxygens.

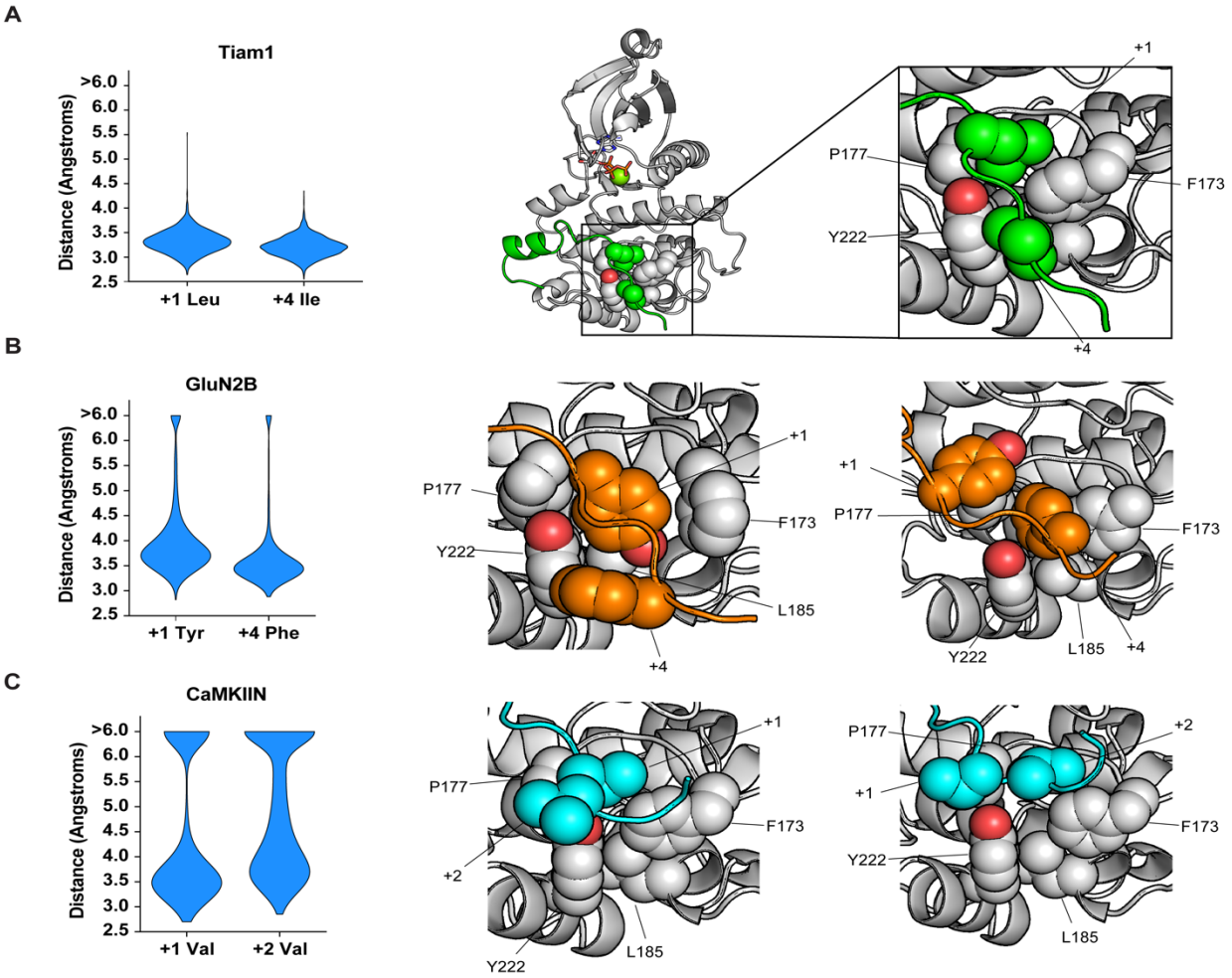

Figure S3. MD simulations highlight a hydrophobic interaction at the C-terminal end of peptides. (A) Persistence of Tiam1 interaction with the F173, P177, L185, Y222 hydrophobic patch in MD simulations. Distance distributions for +1 leucine and +4 isoleucine of Tiam1 to patch (left), representative structure (middle). Zoomed view is labeled for clarity. (B) Persistence of GluN2B interaction with hydrophobic patch. Distance distributions for +1 tyrosine and +4 phenylalanine of GluN2B and two zoomed-in views of the interaction from different orientations. (C) Persistence of CaMKIIN1 interaction with hydrophobic patch from different orientations. Distance distributions for +1 and +2 valine residues of CaMKIIN and two zoomed-in views of the interaction from different orientations.

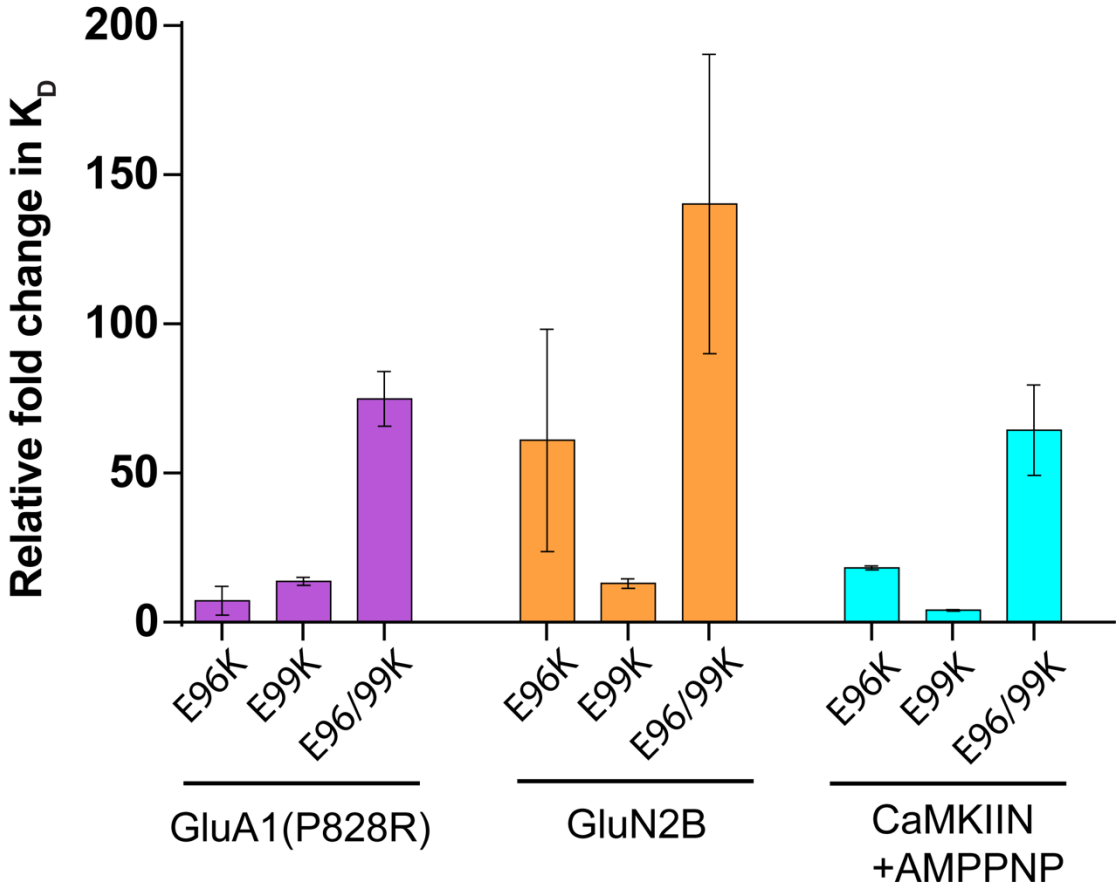

Figure S4. Effect of charge reversal mutations at the -3 position. K_d values were extracted from ITC data and relative fold changes were calculated by dividing the observed K_d from the mutant by the D135N kinase domain. Standard deviations are shown as error bars for duplicate measurements.

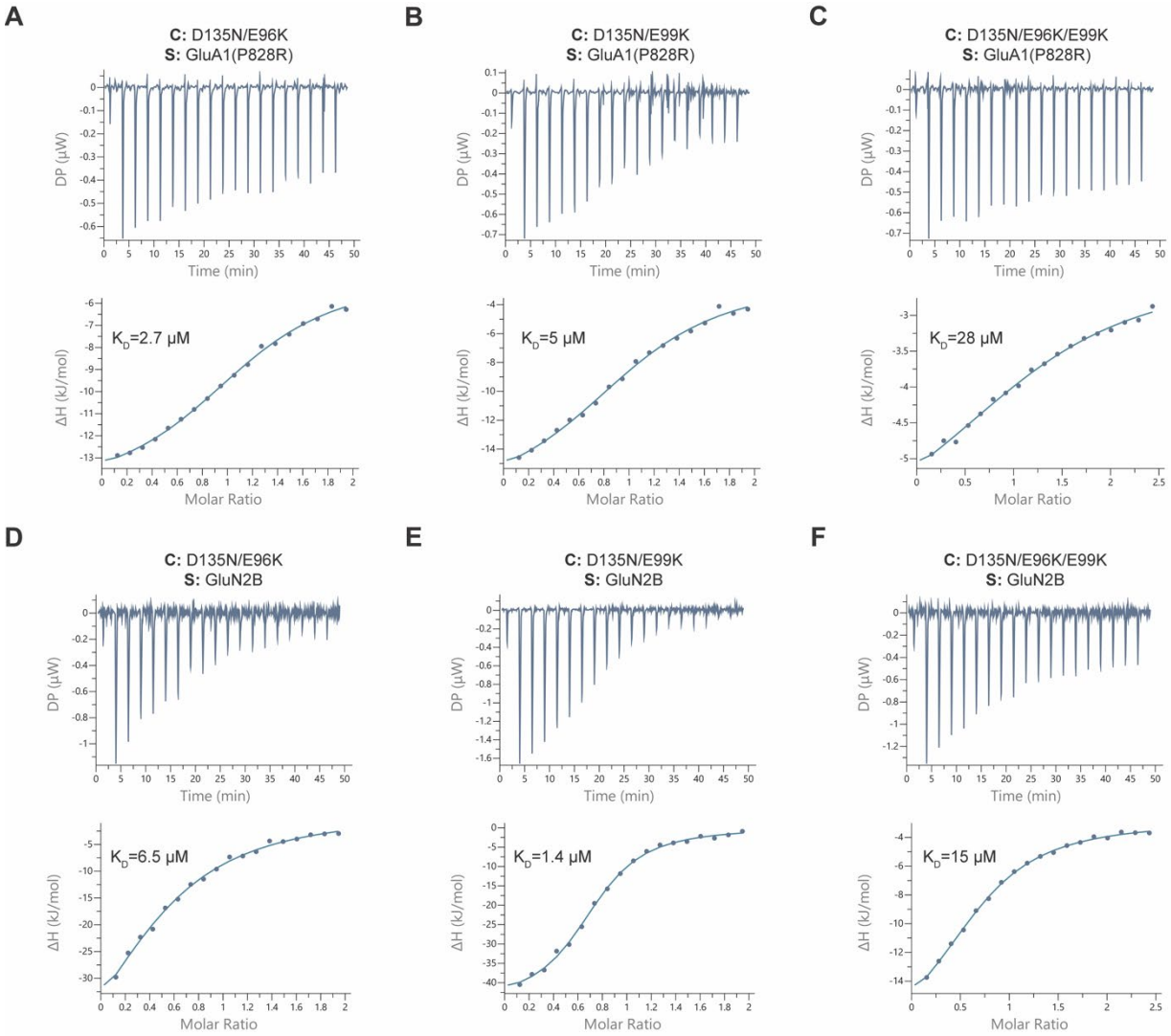

Figure S5. Effect of E96K and E99K mutations on binding affinity. ITC measurements of D135N kinase domain mutants and interaction partners. All measurements were performed in duplicate, here one representative dataset is shown. (A) E96K and GluA1 (P828R), (B) E99K and GluA1 (P828R), (C) E96K/E99K and GluA1 (P828R), (D) E96K and GluN2B, (E) E99K and GluN2B, and (F) E96K/E99K and GluN2B. The mean K_d value from two independent measurements is labeled in the figure.

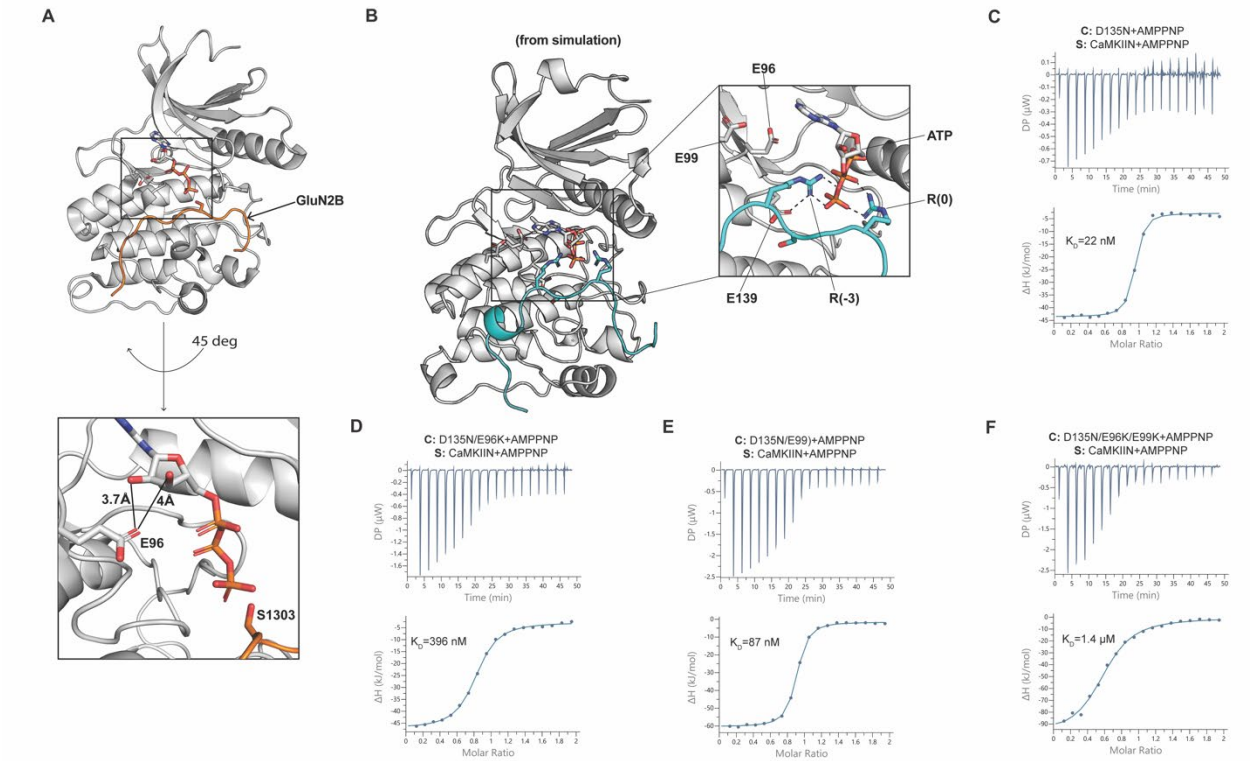

Figure S6. CaMKIIN has unique interactions with ATP. (A) Co-crystal structure of CaMKII kinase domain and GluN2B in complex with ATP (PDB 7UJP). Bottom image highlights the interaction between E96 sidechain and ribose hydroxyl groups of ATP. The gamma phosphate group faces S1303. (B) Snapshot from an MD trajectory with CaMKIIN peptide and ATP bound. The arginine at the -3 position of CaMKIIN mostly interacts with E139, minimally with E96, and not at all with E99. All interactions depicted with dashed lines are below 3 Å. This conformational change precludes the ATP adenosine from forming ionic interactions with the backbones of D90 and V92, as observed in the crystal structure. As a result, the ATP adenosine group exits the binding pocket in the CaMKIIN trajectories. ITC measurements of CaMKIIN in the presence of AMPPNP are shown in C-F. Contents of the cell (C) and syringe (S) used in the ITC measurements are listed in the figure panels. The mean K_d value from two independent measurements is labeled in the figure.

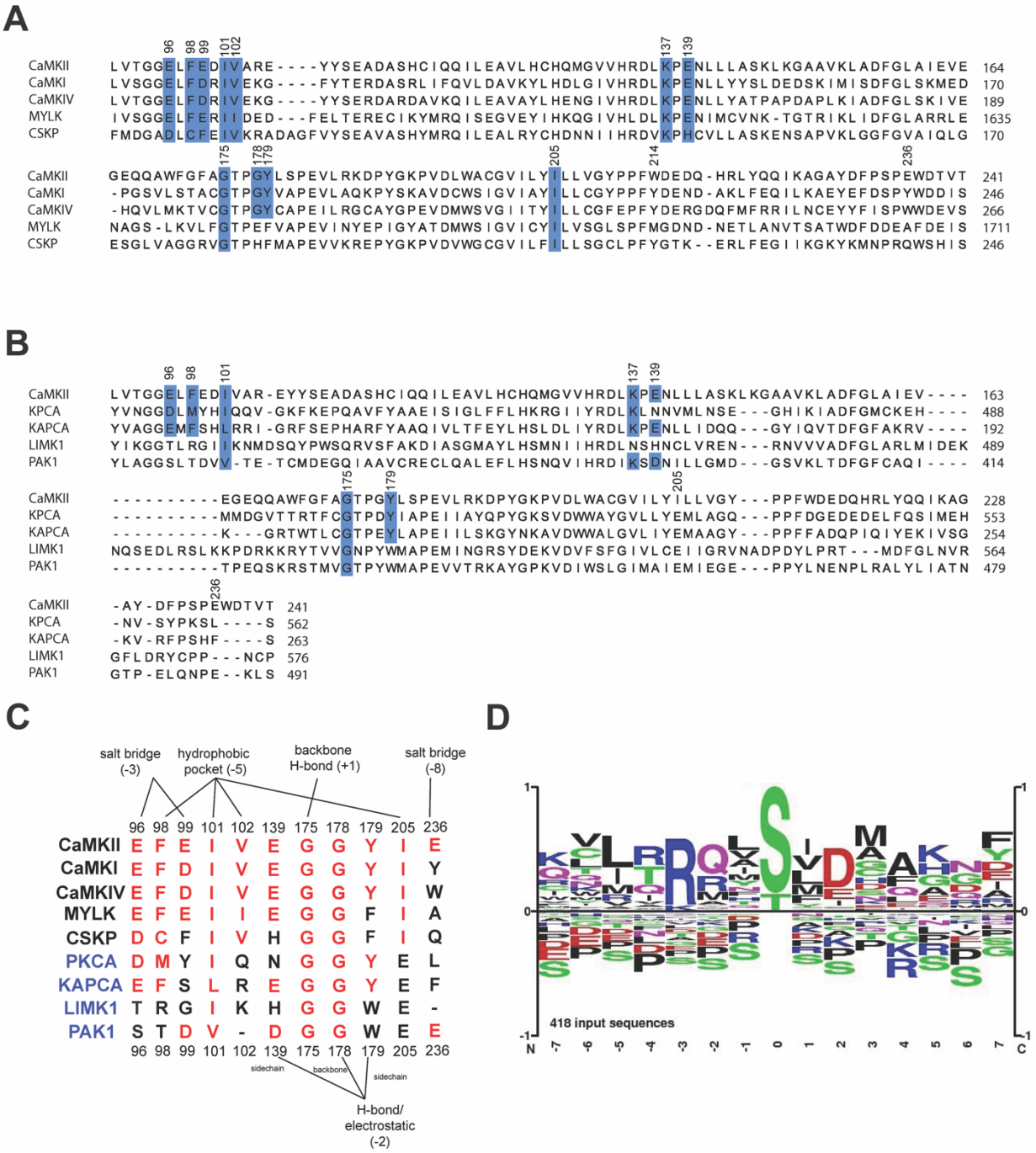

Figure S7. Multi-sequence alignment of kinase domains.
Alignment of CaMKII from residue 91-241 (according to CaMKIIα numbering) is shown (A) across Ca^{2+}/CaM (CaMK) family and (B) across different kinase families. Conserved residues are highlighted blue. (C) Alignment of key residues involved in binding substrates across kinases from the Ca^{2+}/CaM family (black text) and four kinases from different families (blue text). PKCA and KAPCA (cAMP dependent kinase) belong to the AGC Ser/Thr family. LimK1 and Pak1 belong to TKL and STE Ser/Thr family. (D) The sequence logo for all previously identified substrates of CaMKII from the PhosphoSitePlus database with the phosphorylation site at the 0 position.

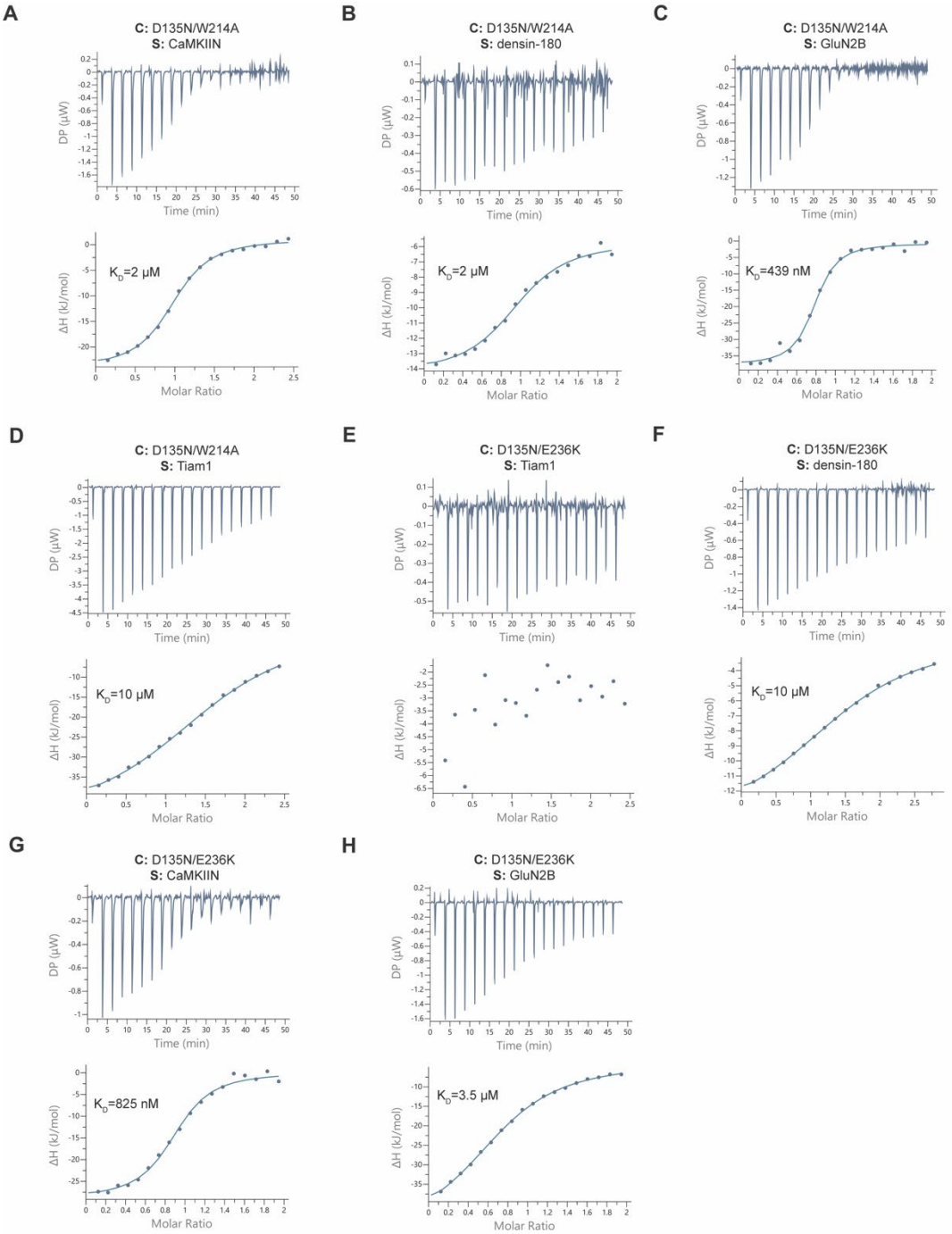

Figure S8. Effect of W214A and E236K mutations on binding affinity. ITC measurements between D135N kinase domain mutants and interaction partners. Contents of the cell (C) and syringe (S) used in the ITC measurements are listed in the figure panels. The mean K_d value from two independent measurements is labeled in the figure.

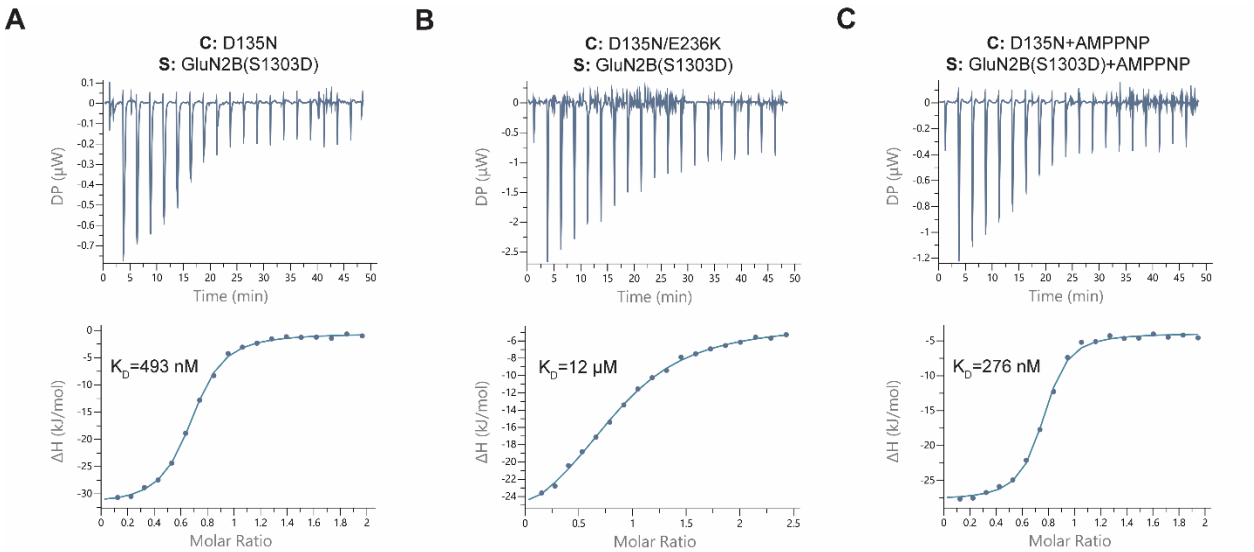

Figure S9. Effect of the phosphomimetic mutation on GluN2B binding affinity. ITC measurements between D135N kinase domain mutants and interaction partners. Contents of the cell (C) and syringe (S) used in the ITC measurements are listed in the figure panels. The mean K_d value from two independent measurements is labeled in the figure.

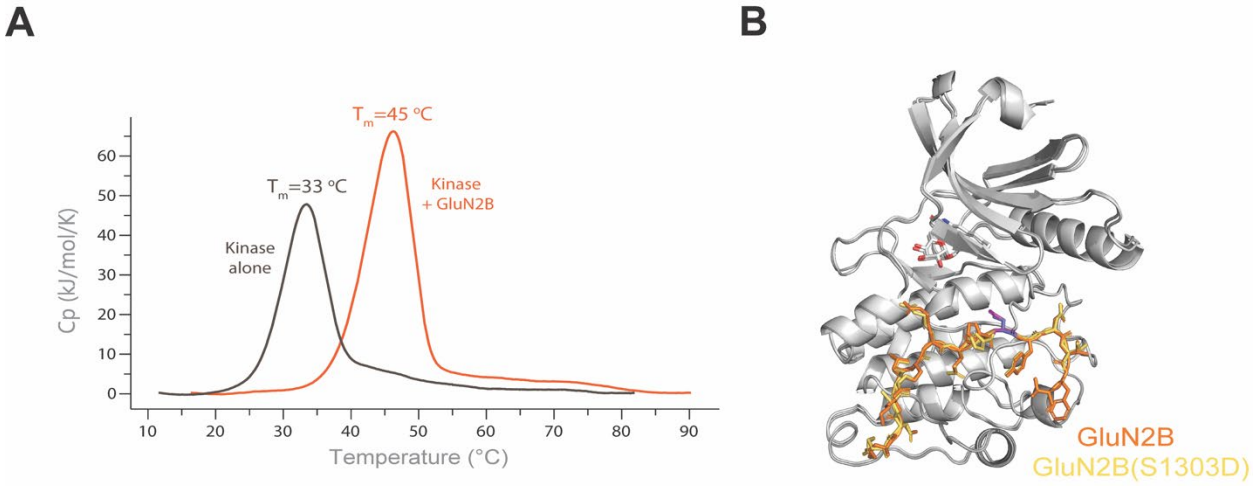

Figure S10. Alignment of WT and S1303D GluN2B bound to the kinase domain and DSC for GluN2B binding.
(A) Differential Scanning Calorimetry data from CaMKII kinase domain alone (brown) and CaMKII kinase domain bound to GluN2B peptide (orange). (B) Overlay of WT and S1303D GluN2B bound kinase domain structures with hecameg bound (detergent present in crystallization condition) (PDB: 7UJQ and 7KL0). The residue at 1303 is highlighted in blue (serine) and magenta (aspartate).

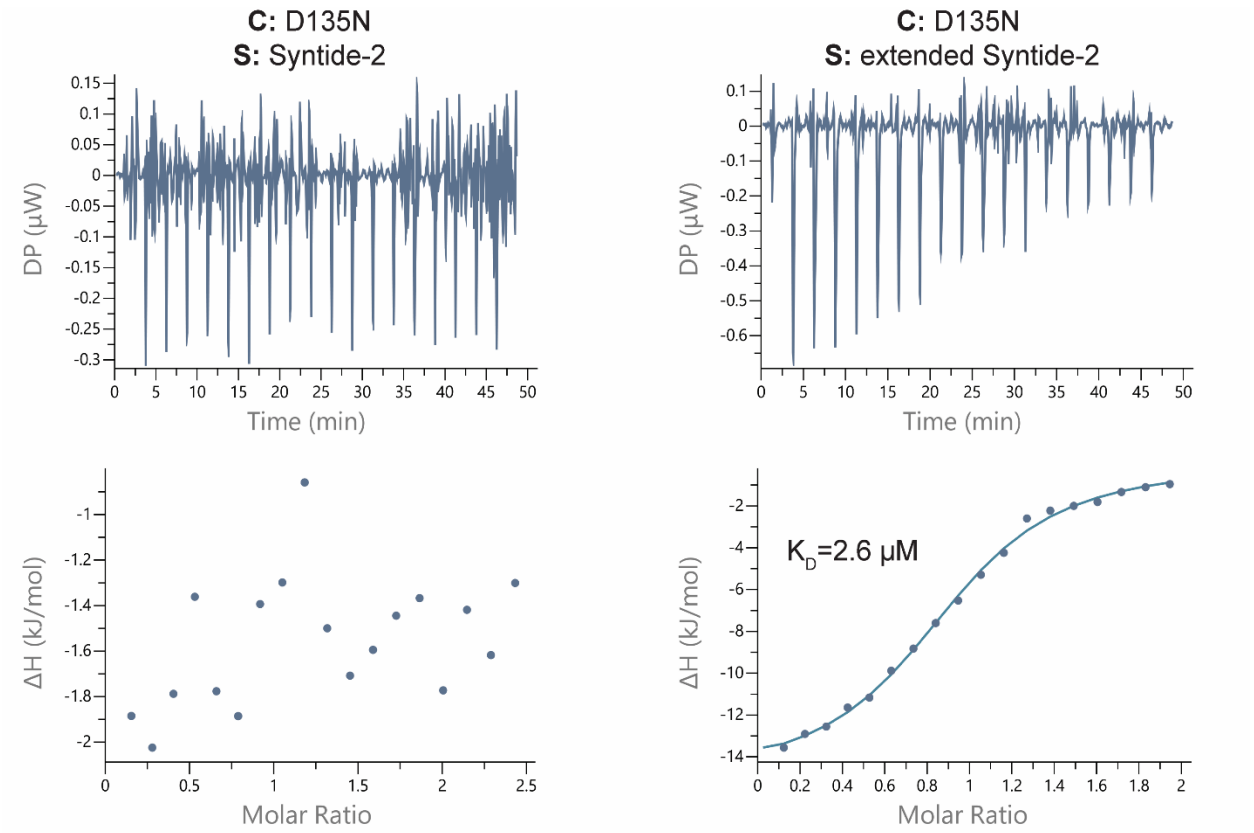

Figure S11. Far salt bridge interaction facilitates low micromolar affinity.
Comparison of Syntide-2 to extended Syntide-2. Contents of the cell (C) and syringe (S) used in the ITC measurements are listed in the figure panels. The mean K_d value from two independent measurements is labeled.

Table 1. GluN2B WT cocrystal structures

	GluN2B/WT kinase/ADP (7UJS)	GluN2B/WT kinase (7UJR)	GluN2B/D135N kinase/ATP (7UJP)	GluN2B/D135N kinase/Hecameg (7UJQ)
Data collection				
Space group	$P12_11$	$P12_11$	$P2_12_12_1$	$P2_12_12_1$
Cell dimensions				
a, b, c (Å)	45.01, 65.23, 53.71	45.09, 66, 45	73.14, 91.42, 91.92	73.25, 91.78, 91.77
α, β, γ (°)	90, 95.26, 90	90, 97.61, 90	90, 90, 90	90, 90, 90
Resolution (Å)	50 – 2.75 (2.85 – 2.8)	50 – 1.95 (1.99 – 1.96)	50 – 2.56 (2.60 – 2.56)	50 – 2.25 (2.29 – 2.25)
R_{merge}	0.102 (0.374)	0.13 (0.485)	0.232 (0.812)	0.116 (0.374)
Mean $I/\sigma I$	5 (1.57)	9.5 (2)	5 (1.86)	9.3 (4.36)
Completeness (%)	93.8 (90.9)	93.8 (82.7)	100 (99.8)	96.9 (90.1)
Redundancy	2.6 (2.5)	2.7 (2.5)	6.3 (5.4)	6.3 (5.7)
$CC_{1/2}$	0.985 (0.711)	0.956 (0.678)	0.976 (0.572)	0.99 (0.868)
CC*	0.996 (0.912)	0.989 (0.899)	0.994 (0.853)	0.997 (0.964)
Refinement				
Resolution (Å)	44.86 – 2.75 (2.82 – 2.75)	33.92 – 1.95 (2.00 – 1.95)	48-56 – 2.56 (2.62 – 2.56)	45.93 – 2.25 (2.31 – 2.25)
Unique reflections	7103 (428)	16929 (1027)	19465 (1411)	27648 (1847)
R_{work} / R_{free} (%)	22.28/25.56	20.93/25.16	23.18/28.08	21.99/27.11
No. atoms				
Protein	2253	2234	4479	4507
Water	-	93	45	129
Ligand	27	17	67	52
Ramachadran plot				
In preferred regions (%)	93.57	96.03	96.93	95.85
In allowed regions (%)	5.71	3.97	3.07	3.79
Outliers (%)	0.71	0.0	0.0	0.36
B-factors				
Protein	38.04	30.62	32.74	27.15
Water	-	33.63	18.61	21.49
Ligand	71.96	45.15	48.55	23.01
R.m.s. deviations				
Bond lengths (Å)	0.0033	0.0021	0.0037	0.0028
Bond angles (°)	1.2665	1.11809	1.2648	1.2374

Table 2. GluN2B S1303D cocrystal structures

	GluN2B(S1303D) /D135N kinase/ATP (7KL1)	GluN2B(S1303D) /D135N kinase/ATP (7UJT)	GluN2B(S1303D) /D135N kinase (PDB 7UIS)	GluN2B(S1303D) /D135N kinase/Hecameg (7KL0)
Data collection				
Space group	$P2_12_12_1$	$P12_11$	$P12_11$	$P2_12_12_1$
Cell dimensions				
a, b, c (Å)	72.89, 92.13, 91.34	47.31, 67.25, 45.72	43.41, 71.43, 45.28	72.99, 91.29, 92.08
α, β, γ (°)	90, 90, 90	90, 94.43, 90	90, 97.51, 90	90, 90, 90
Resolution (Å)	50 – 2.4 (2.44 – 2.4)	50 – 2.1 (2.14 – 2.1)	50 – 2.58 (2.64 – 2.6)	50-2.4 (2.44-2.4)
R_{merge}	0.183 (0.527)	0.098 (0.297)	0.162 (0.678)	0.188 (0.627)
Mean $I/\sigma I$	5.9 (2.65)	9.9 (3.51)	5.8 (1.52)	4.9 (2.04)
Completeness (%)	99.9 (98.8)	99.6 (97.3)	96.9 (92.5)	99.9 (99.5)
Redundancy	5.7 (5)	3.3 (2.8)	3.3 (3.4)	5.6 (4.9)
$CC_{1/2}$	0.976 (0.740)	0.993 (0.824)	0.977 (0.743)	0.984 (0.652)
CC*	0.994 (0.922)	0.998 (0.951)	0.994 (0.658)	0.996 (0.888)
Refinement				
Resolution (Å)	48.5 – 2.4 (2.46 – 2.4)	38.65 – 2.1 (2.15 – 2.1)	24.37 – 2.58 (2.65 – 2.58)	48.52 – 2.4 (2.46 – 2.4)
Unique reflections	23497 (1650)	15852 (1096)	7962 (502)	23396 (1610)
R_{work} / R_{free} (%)	20.60/25.75	20.34/24.65	21.73/ 26.75	20.71/25.84
No. atoms				
Protein	4524	2268	2207	4497
Water	118	96	0	131
Ligand	76	38	0	54
Ramachadran plot				
In preferred regions (%)	97.12	95.71	95.64	96.74
In allowed regions (%)	2.88	3.93	4.36	3.26
Outliers (%)	0.0	0.36	0.0	0.0
B-factors				
Protein	28.11	28.27	43.53	25.95
Water	20.96	28.26	-	20.24
Ligand	32.40	41.33	-	26.08
R.m.s. deviations				
Bond lengths (Å)	0.0074	0.0021	0.0030	0.0073
Bond angles (°)	1.4853	1.1765	1.2691	1.4717

Table 3. Tiam1, Densin-180 and GluA1 cocrystals structures

	Tiam1/D135N kinase/ATP (7UIR)	Tiam1/D135N kinase (7UIQ)	Densin-180/D135N kinase (PDB 6X5G)	GluA1/D135N kinase (6X5Q)
Data collection				
Space group	$P2_12_12_1$	$P2_12_12_1$	$P12_11$	$P2_12_12_1$
Cell dimensions				
a, b, c (Å)	43.49, 138.84, 154.97	43.43, 137.42, 156.47	36.29, 66.17, 61.71	42.63, 57.46, 107.71
α, β, γ (°)	90, 90, 90	90, 90, 90	90, 99.78, 90	90, 90, 90
Resolution (Å)	50 – 3.1 (3.18 – 3.13)	50 – 3.11 (3.17 – 3.12)	50 - 1.85 (1.88-1.85)	50 – 2.1 (2.18 - 2.14)
R_{merge}	0.287 (0.87)	0.266 (0.67)	0.065 (0.325)	0.179 (0.377)
Mean $I/\sigma I$	3.9 (1.47)	3.9 (1.53)	9.6 (3.14)	3.2 (2.21)
Completeness (%)	98 (96.5)	93.4 (91.9)	93.6 (86.5)	96.9 (92.7)
Redundancy	5.6 (4.6)	4.6 (3.5)	3.4 (3.3)	4.9 (4.4)
$CC_{1/2}$	0.975 (0.618)	0.992 (0.565)	0.99 (0.829)	0.992 (0.82)
CC*	0.994 (0.831)	0.969 (0.831)	0.997 (0.952)	0.998 (0.949)
Refinement				
Resolution (Å)	33.31 – 3.1 (3.183 – 3.103)	31.54 – 3.11 (3.20 – 3.12)	33.11 - 1.85 (1.895-1.85)	39.32 – 2.14 (2.159 – 2.104)
Unique reflections	16512 (1130)	15535 (1042)	22043 (1457)	14475 (798)
R_{work} / $R_{free\ (\%)}$	23.21/27.44	25.85/30.92	18.71/22.65	18.93/23.5
No. atoms				
Protein	4438	4430	2259	2241
Water	0	0	107	96
Ligand	79	0	23	18
Ramachadran plot				
In preferred regions (%)	93.48	91.11	97.48	95.71
In allowed regions (%)	5.62	8.17	2.52	4.29
Outliers (%)	0.91	0.73	0.0	
B-factors				
Protein	45.73	33.76	24.09	17.35
Water	-	-	25.19	14.48
Ligand	62.04	-	53.79	30.61
R.m.s. deviations				
Bond lengths (Å)	0.0052	0.0068	0.0096	0.0080
Bond angles (°)	1.4030	1.5793	1.6299	1.5184

Table 4: ITC data 1

Cell	Syringe	K_D (μM)	N	ΔH (kJ/mol)	-TΔS (kJ/mol)	[Cell]/[Syringe] (μM)
D135N	GluN2B	$107 \times 10^{-3} \pm 47 \times 10^{-3}$	0.79±0.03	-45.35±0.21	6.06±0.86	20/200
D135N	Tiam1	$1.1 \pm 28 \times 10^{-3}$	0.8±0.02	-88.15±1.77	54.7±1.7	20/200
D135N	densin-180	$586 \times 10^{-3} \pm 114 \times 10^{-3}$	0.79±0.02	-32.05±1.49	-2.9±2	20/200
D135N	GluA1	58±28	0.99±0.2	-18.6±8.2	-5.34±9.42	40/500
D135N	CaMKIIN	$39 \times 10^{-3} \pm 24 \times 10^{-3}$	0.98±0.02	-30.9±2.97	-10.94±4.61	20/200
D135N	Syntide-2	ND	ND	ND	ND	40/500
D135N	Extended Syntide-2	2.6±0.9	0.89±0.02	-16.45±1.91	-15.05±2.76	20/200
D135N/E96K	GluN2B	6.5±4	0.58±0.08	-50.15±15.91	20.74±17.49	20/200
D135N/E99K	GluN2B	1.4±0.2	0.72±0.01	-45.6±0.71	12.75±0.35	20/200
D135N/EE96/99KK	GluN2B	15±5	0.64±0.0007	-19.6±4.95	-7.58±5.82	40/500
D135N/W214A	GluN2B	$439 \times 10^{-3} \pm 120 \times 10^{-3}$	0.76±0.01	-39.05±2.76	3.3±3.5	20/200
D135N+AMPPNP	GluN2B (S1303D)+ AMPPNP	$277 \times 10^{-3} \pm 30 \times 10^{-3}$	0.73±0.008	-25.2±1.84	-11.7±2.12	20/200
D135N	GluN2B (S1303D)	$493 \times 10^{-3} \pm 47 \times 10^{-3}$	0.62±0.05	-32±0.71	-3.55±0.76	20/200
D135N/E236K	GluN2B	3.5±1	0.83±0.1	-39.4±6.51	8.72±7.18	20/200
D135N/E236K	GluN2B (S1303D)	12±4.5	0.85±0.009	-28.85±4.46	1.08±5.41	40/500

n=2 for each measurement.

Table 5: ITC data 2

Cell	Syringe	K_D (μM)	N	ΔH (kJ/mol)	-TΔS (kJ/mol)	[Cell]/[Syringe] (μM)
D135N+AMPPNP	CaMKIIN+ AMPPNP	$22x10^{-3}\pm4x10^{-3}$	0.91±0.007	-40.7±0.14	-2.35±0.52	8/80
D135N/E96K +AMPPNP	CaMKIIN+ AMPPNP	$397x10^{-3}\pm 15x10^{-3}$	0.79±0.008	-43±2.12	7.06±2.19	20/200
D135N/E99K +AMPPNP	CaMKIIN+ AMPPNP	$87x10^{-3}\pm12x10^{-3}$	0.86±0.004	-58.8	19.15±0.35	20/200
D135N/EE96/99KK +AMPPNP	CaMKIIN+ AMPPNP	1.4±0.3	0.58±0.01	-103.8±7.43	70.65±7.7	20/200
D135N/E236K	CaMKIIN	$825x10^{-3}\pm6x10^{-3}$	0.87±0.02	-29.65±0.78	-4.53±0.76	20/200
D135N/W214A	CaMKIIN	2±0.2	0.97±0.007	-25.05±0.21	6.57±0.4	40/500
D135N/W214A	Tiam1	10±4	1.56±0.1	-43.7±5.8	15.55±6.72	40/500
D135N/E236K	Tiam1	ND	ND	ND	ND	40/500
D135N/W214A	densin-180	2±0.7	0.98±0.006	-10.07±2.03	-21.9±2.83	20/200
D135N/E236K	densin-180	10±7	1.36±0.25	-11.14±2.07	-17.25±3.75	35/500
D135N	GluA1 (P828R)	$376x10^{-3}\pm110x10^{-3}$	1.17±0.04	-23.4±1.41	-12.7±2.12	20/200
D135N/E96K	GluA1 (P828R)	2.7±1.8	1.06±0.14	-8.08±2.54	-23.55±4.31	20/200
D135N/E99K	GluA1 (P828R)	5±0.5	1.33±0.4	-15.9±0.57	-13.8±0.71	20/200
D135N/EE96/99KK	GluA1 (P828R)	28±3	1.22±0.16	-4.52±0.79	-21.05±1.06	40/500

n=2 for each measurement.